African horse sickness virus infects BSR cells through macropinocytosis

Elaine Vermaak[a], Andelé M. Conradie[a], Francois F. Maree[a,b] and Jacques Theron[a]*

[a] Department of Microbiology and Plant Pathology, University of Pretoria, Pretoria 0002, South Africa

[b] Transboundary Animal Diseases, Onderstepoort Veterinary Institute, Agricultural Research Council, Pretoria 0110, South Africa

***Corresponding author:** Prof Jacques Theron
Email: jacques.theron@up.ac.za
Telephone: +27 12 420-2994
Fax: +27 12 420-3266

Highlights

- AHSV entry requires endocytic vesicle acidification.
- AHSV enters cells via a caveolin- and clathrin-independent pathway.
- An entry pathway involving a macropinocytosis-like entry mechanism is proposed.

ABSTRACT

Cellular pathways involved in cell entry by African horse sickness virus (AHSV), a member of the *Orbivirus* genus within the *Reoviridae* family, have not yet been determined. Here, we show that acidic pH is required for productive infection of BSR cells by AHSV-4, suggesting that the virus is likely internalized by an endocytic pathway. We subsequently analyzed the major endocytic routes using specific inhibitors and determined the consequences for AHSV-4 entry into BSR cells. The results indicated that virus entry is dynamin dependent, but clathrin- and lipid raft/caveolae-mediated endocytic pathways were not used by AHSV-4 to enter and infect BSR cells. Instead, binding of AHSV-4 to BSR cells stimulated uptake of a macropinocytosis-specific cargo and inhibition of Na^+/H^+ exchangers, actin polymerization and cellular GTPases and kinases involved in macropinocytosis significantly inhibited AHSV-4 infection. Altogether, the data suggest that AHSV-4 infects BSR cells by utilizing macropinocytosis as the primary entry pathway.

Keywords

African horse sickness virus; orbivirus; endocytosis; macropinocytosis; cell entry

Introduction

The initial steps in viral infection involve the attachment of the virion to a receptor(s) on the cell surface, followed by internalization of the virus into the cell and subsequent uncoating of the virion to release the active transcription complex. Several distinct internalization pathways exist in mammalian cells that can be used by viruses to enter cells. These pathways are distinguished from each other on a number of criteria, including the mechanism of vesicle formation, the size of the endocytic vesicles, the type of cargo they carry and the transport route of the vesicles (Sieczkarski and Whittaker, 2002; Doherty and McMahon, 2009; Mercer et al., 2010b; Mercer and Helenius, 2012).

Clathrin-mediated endocytosis is the best understood endocytic pathway. A number of viruses, including Semliki Forest virus, vesicular stomatitis virus, bluetongue virus (BTV) and rabies virus, make use of this endocytic pathway for internalization and productive

infection (Helenius et al., 1980; Sun et al., 2005; Forzan et al., 2007; Piccinotti et al., 2013). Clathrin-mediated endocytosis is characterized by the formation of clathrin-coated pits on the cytoplasmic face of the plasma membrane that bud into the cytoplasm to form clathrin-coated vesicles. These vesicles are approximately 120 nm in diameter and contain the internalized cargo (Doherty and McMahon, 2009). The cargo is subsequently delivered to mildly acidic early endosomes, from where they are sorted for transport to either late endosomes or lysosomes for degradation, or to recycling endosomes for recycling back to the cell surface (Marsh and Helenius, 2006; McMahon and Boucrot, 2011).

Caveolae-mediated endocytosis was first observed for the cellular uptake of simian virus 40 (Kartenbeck et al., 1989) and a number of viruses has since been reported to enter cells via this pathway (Moriyama et al., 2007; O'Donnell et al., 2008; Huang et al., 2011). Caveolae are flask-shaped invaginations in the plasma membrane, which have an average diameter of approximately 50-80 nm. Caveolae are rich in caveolin protein and are predominantly associated with cholesterol-rich plasma membrane microdomains, termed lipid rafts (Parton, 2003; Parton and Simons, 2007). Cargoes internalized by caveolae pass through a series of endocytic organelles (early endosomes, late endosomes and endolysosomes) and are trafficked to the endoplasmic reticulum or Golgi (Hayer et al., 2010; Engel et al., 2011). Although several viruses use caveolae for infection, a number of caveolin-independent pathways also originate from lipid rafts that can be exploited by viruses for infection (Gerondopoulos et al., 2010; Nonnenmacher and Weber, 2011; Garcin and Panté, 2015).

The importance of macropinocytosis, as a distinct endocytic uptake mechanism for virus infection, has been reported for some viruses, including vaccinia virus (Mercer and Helenius, 2008), adenovirus (Kalin et al., 2010), BTV (Gold et al., 2010), Ebola virus (Saeed et al., 2010) and influenza virus (de Vries et al., 2011). Macropinocytosis is associated with membrane ruffles such as those formed by filopodia and lamellipodia, which are outward extensions of the plasma membrane driven by actin polymerization underneath the membrane surface. When a ruffle folds back on itself a cavity can be formed and subsequent fusion with the plasma membrane results in the formation of a large vesicle called a macropinosome, which can range in size from 0.2-5 μm in diameter (Swanson, 2008). The macropinosomes are dynamic structures and are able to transport internalized cargo through the cortical cytoskeleton and cytoplasm (Mercer and Helenius, 2012).

The present study investigated the entry route used by African horse sickness virus (AHSV) to infect BSR mammalian cells. AHSV is a member of the *Orbivirus* genus within the *Reoviridae* family and is the aetiological agent of African horse sickness, a vector-borne disease of equids that can cause up to 90% mortality in susceptible horses (Stassen et al., 2014). The virion is comprised of two concentric protein layers that enclose the genome of ten double-stranded RNA (dsRNA) segments. The core particle is composed of two major (VP3 and VP7) and three minor (VP1, VP4 and VP6) structural proteins, and is surrounded by the outer capsid, composed of the two major structural proteins VP2 and VP5 (Manole et al., 2012). The outermost capsid protein VP2 is associated with cell binding, whereas the less exposed VP5 protein is involved in cell membrane permeabilization (Hassan and Roy, 1999; Hassan et al., 2001; Stassen et al., 2011). The outer capsid proteins are removed during cell entry, and the transcriptionally active core particles are released into the cytoplasm of infected cells where viral replication occurs (Forzan et al., 2007). As infection progresses viral inclusion bodies (VIBs), directed by non-structural protein NS2, begin to form and act as sites for virus replication and early viral assembly (Uitenweerde et al., 1995; Kar et al., 2007).

The molecular-genetic events underlying the infectious cycle of AHSV remains poorly defined and the first step in a productive infection, i.e. the mechanism of AHSV entry into mammalian cells, has not yet been characterized. In this report, we show that exposure of AHSV-4 to acidic pH is required for productive infection. A combination of pharmacological, biochemical and microscopy approaches were then used to study the entry and infection of BSR cells by AHSV-4. The results indicate that AHSV-4 enters and infects BSR cells by an endocytic mechanism that fits criteria defining macropinocytosis.

Results

AHSV-4 infection of BSR cells requires active endosomal acidification

Previous reports have shown that infection of cells by BTV, the prototype Orbivirus species, is dependent on a low endosomal pH (Forzan et al., 2007). To determine whether a low endosomal pH is required for AHSV-4 infection, BSR cells were exposed to two inhibitors of endosomal acidification, i.e. ammonium chloride (AC) and chloroquine (CQ), and their effect was examined at 24 h post-infection. Infected cells were identified with an antibody that

binds the viral NS2 protein (a marker of virus replication) and a FITC-conjugated secondary antibody. Pre-treatment of BSR cells with the lysosomotropic drugs inhibited AHSV-4 infection and a similar strong inhibitory effect was also observed when the drugs were added coincident with the start of infection. When the drugs were added 2 h after infection was initiated, the frequency of infection was reduced by 38% in AC-treated cells and by 57% in CQ-treated cells when compared to mock-treated BSR cells (Fig. 1). These results thus indicate that, like BTV, endosomal acidification is important in AHSV-4 internalization and suggests that the virus is likely internalized by an endocytic pathway.

Infection of BSR cells by AHSV-4 does not require clathrin-mediated endocytosis

To evaluate the role of clathrin-dependent endocytosis in AHSV-4 entry and infection of BSR cells, we tested the effect of treating BSR cells with chlorpromazine (CPZ), which prevents the assembly of clathrin-coated pits at the plasma membrane (Wang et al., 1993; Palacios et al., 1993), or with a hypertonic medium (0.45 M sucrose), which results in the dissociation of clathrin vesicles from the plasma membrane (Heuser and Anderson, 1989; Hansen et al., 1993).

The effectiveness of these treatments for inhibition of clathrin-mediated endocytosis was first tested by determining the ability of treated BSR cells to endocytose Alexa-568-labelled transferrin, which is generally used as a marker for clathrin-mediated endocytosis. In contrast to mock-treated cells, transferrin internalization was inhibited in cells treated with CPZ (5 µM) or sucrose (0.45 M) (Fig. 2A). The effect of these inhibitors on AHSV-4 infection was subsequently determined by infection of BSR cells that were pre-treated with CPZ or sucrose for 30 min at 37°C and then infected with AHSV-4 at a MOI of 1 pfu/cell for 24 h in the presence of the respective inhibitors. At this time point, the cells were fixed and infected cells were identified by confocal microscopy using an anti-NS2 antibody as described above. The results indicated that these treatments had no apparent effect on the ability of AHSV-4 to infect cells compared to virus infection of mock-treated cells (Figs. 2B and 2C). We next examined the effects of different concentrations of CPZ and 0.45 M sucrose on virus titres obtained from cell cultures 24 h after infection. Treatment of BSR cells with these inhibitors did not affect virus progeny production (Fig. 2D). The virus titre of cells treated with 10 µM CPZ (2.0×10^5 pfu/ml) or 0.45 M sucrose (1.9×10^5 pfu/ml) were similar to that of mock-treated cells (2.1×10^5 pfu/ml). Moreover, immunoblot analysis indicated that synthesis of

the viral VP5 protein was not inhibited by these treatments (Fig. 2E). These results thus indicate that AHSV-4 is capable of entering and infecting BSR cells lacking a functional clathrin-mediated endocytosis pathway.

Infection of BSR cells by AHSV-4 does not require cholesterol-dependent endocytic pathways

To determine whether AHSV-4 enters BSR cells through a lipid raft/caveolae-mediated endocytic pathway, cells were treated with drugs that are known to inhibit this pathway and subsequently infected with AHSV-4. Caveolae-mediated endocytosis is dependent on the integrity of lipid rafts, of which cholesterol is a prominent component, and like other lipid raft-mediated endocytic pathways can be inhibited by cholesterol depletion or sequestration (Sieczkarski and Whittaker, 2002; Lajoie and Nabi, 2010).

The effect of cholesterol depletion on AHSV-4 infection was investigated by making use of methyl-β-cyclodextrin (MβCD), which binds and extracts cholesterol from the plasma membrane. BSR cells were mock-treated or treated with MβCD (2 µg/ml) for 30 min and then incubated with filipin, which binds cholesterol and can be detected by fluorescence microscopy. Although filipin fluorescence was detected within the cytoplasm of treated cells, the intense plasma membrane fluorescence generated by filipin binding in mock-treated cells was greatly reduced in cells treated with MβCD, thus indicating extensive and selective cholesterol depletion from the cell surfaces (Fig. 3A). Subsequently, BSR cells were pre-treated with MβCD and then infected with AHSV-4 at a MOI of 1 pfu/cell in the presence of the drug. At 24 h post-infection the cells were processed for confocal microscopy using NS2 to detect infected cells. The results indicated that MβCD did not inhibit virus infection when compared to infected mock-treated cells (Figs. 3B and 3C). Near identical results were obtained in an alternative assay using nystatin in place of MβCD (Figs. 3B and 3C). Nystatin sequesters membrane cholesterol, disrupts membrane lipid rafts and thus prevents caveolae formation (Rothberg et al., 1992; Smart and Anderson, 2002). Additional data acquired from virus titration and immunoblotting indicated that neither progeny virus production nor VP5 protein synthesis was affected in BSR cells treated with different concentrations of these drugs (Figs. 3D and 3E). Similar virus titres were obtained from cells treated with 2 µg/ml MβCD (2.4×10^5 pfu/ml) or 80 µg/ml nystatin (2.2×10^5 pfu/ml) and mock-treated cells (2.5×10^5 pfu/ml). Collectively, the results indicate that AHSV-4 infection of BSR cells does not

require cholesterol and thus the cell entry mechanism used by AHSV-4 to infect BSR cells is unlikely to be mediated by lipid-rafts or caveolae-mediated endocytic pathways.

Infection of BSR cells by AHSV-4 is dependent on cellular dynamin

Dynamin is a large GTPase that is required for phagocytosis and caveolae-mediated and clathrin-mediated endocytosis, as well as for some clathrin- and caveolae-independent endocytosis pathways (Hinshaw, 2000; Doherty and McMahon, 2009; Gold et al., 2010; Khan et al., 2011; Mulherkar et al., 2011; Sánchez et al., 2012). To investigate the involvement of dynamin in AHSV-4 entry and infection, the effect of dynasore, a potent and specific dynamin inhibitor (Macia et al., 2006), was tested. To ensure that dynasore inhibited dynamin-mediated endocytosis, its effect on internalization of transferrin (clathrin-mediated endocytosis marker) and dextran (macropinocytosis marker) was determined (Fig. 4A). Confocal microscopy revealed that treatment of the cells with 100 µM dynasore reduced internalization of both markers by 98% and 97%, respectively, in BSR cells (at least 200 cells counted in each of two independent experiments). The effect of dynasore on AHSV-4 infection was subsequently assayed using an experimental approach similar to that described above. In contrast to mock-treated cells, considerably less NS2 staining was seen in cells infected with AHSV-4 in the presence of dynasore (Fig. 4B). Dynasore treatment of the cells reduced AHSV-4 infection by 64% compared to mock-treated cells infected with AHSV-4 (Fig. 4C). To further analyze a possible role for dynamin during AHSV-4 infection, BSR cells were treated with dynasore at different concentrations prior to infection with AHSV-4. In the presence of dynasore the progeny virus titres of AHSV-4 was reduced in a dosage dependent manner. Compared to mock-treated cells (1.82×10^5 pfu/ml), the virus titres from cells treated with 25, 50 and 100 µM dynasore were 1.3×10^5, 6.8×10^4 and 3.3×10^4 pfu/ml, respectively (Fig. 4D). Likewise, viral VP5 protein synthesis was also diminished by dynasore in a dose-dependent manner (Fig. 4E). These results suggest that AHSV-4 entry into BSR cells for productive infection is dynamin dependent.

Ultrastructural analysis of AHSV-4 internalization by BSR cells

Since the data indicated that AHSV-4 internalization was not affected by the inhibition of clathrin- or lipid raft/caveolae-mediated endocytosis, we next investigated whether AHSV used macropinocytosis to enter BSR cells. For this purpose, the uptake of AHSV-4 by BSR

cells was studied by electron microscopy. At 15 min post-infection of the cells with AHSV-4, extensive ruffle formation was detected on the surface of BSR cells and virus particles were visible on the cell surface next to elongated cellular protrusions resembling membrane blebs or ruffles (Fig. 5A). At 15 and 30 min post-infection, cup-like indentations were observed at the cell surface and viruses were seen in the process of engulfment by large cell extensions that started to embrace virus particles (Fig. 5B). Examination of the infected cells at 1 h post-infection indicated the presence of large smooth-surfaced endocytic vesicles under the plasma membrane that resembled macropinosomes with diameters of *ca*. 0.8-0.85 µm (Fig. 5C). As shown in Fig. 5D, ruffle formation was not observed in mock-infected BSR cells or in cells that had been pre-treated and infected with AHSV-4 in the presence of 5-(N-ethyl-N-isopropyl)-amiloride (EIPA), a known inhibitor of macropinocytosis (Koivusalo et al., 2010).

Due to the high amount of cell ruffling and the large size of the endocytic vesicles, the induction of fluid phase uptake by AHSV-4 infection was next studied. The hallmark of macropinocytosis activation is fluid phase uptake; viruses that enter cells via macropinocytosis have been shown to enhance this fluid-phase uptake (Mercer and Helenius, 2009). To investigate, BSR cells were infected with AHSV-4 in the presence or absence of the fluid phase marker horseradish peroxidase (HRP). Examination of thin sections of infected cells by electron microscopy showed the presence of AHSV-4 virus particles within HRP-labeled structures (Fig. 5E), and measurements of HRP activity showed that there was a marked increase (5.6-fold) in the uptake of HRP in cells infected with AHSV-4 (Fig. 5F).

The above results indicate that AHSV-4 uptake in BSR cells occurs through a pathway that has characteristics of macropinocytosis.

Inhibitors of macropinocytosis interfere with AHSV-4 internalization into BSR cells

Macropinocytosis is heavily dependent on actin, which is required for the formation of plasma membrane ruffles in macropinosome formation as well as trafficking macropinosomes into the cell (Doherty and McMahon, 2009; Mercer et al., 2010b). Macropinocytosis is also dependent on the amiloride-sensitive Na^+/H^+ exchangers that are important for macropinosome formation (Kerr and Teasdale, 2009; Mercer and Helenius, 2009). Consequently, to generate biochemical evidence in support of the role of

macropinocytosis in productive AHSV-4 infection, various inhibitors and their effect on virus uptake were assessed.

We first investigated whether AHSV-4 entry into BSR cells requires actin by making use of cytochalasin D, which disrupts actin filaments (Schliwa, 1982; Goddette and Frieden, 1986). The activity of cytochalasin D was assessed by using Alexa-568-labelled phalloidin to stain BSR cells treated with cytochalasin D (5 µg/ml). As shown in Fig. 6A, the actin network was disassembled in these cells. Mock-treated or cytochalasin D-treated cells were subsequently allowed to internalize AHSV-4 in the presence of cytochalasin D. At 24 h post-infection, cells were processed for confocal microscopy using the anti-NS2 antibody to detect infected cells. Cytochalasin D effectively blocked entry of AHSV-4 and an 81% reduction in NS2-expressing cells was observed in drug-treated cells compared to virus-infected mock-treated cells (Figs. 6B and 6C). Moreover, incubation of the BSR cells with different concentrations of cytochalasin D resulted in a strong inhibitory effect on progeny virus titres of AHSV-4. The progeny virus titre was reduced to 2.9×10^3 pfu/ml for cells treated with 5 µg/ml of the drug as compared to 1.72×10^5 pfu/ml for the mock-treated cells. Likewise, cytochalasin D showed a marked inhibitory effect on viral VP5 protein synthesis (Figs. 6D and 6E). These results thus indicate that AHSV-4 uptake by BSR cells is actin dependent.

Subsequently, the effect of EIPA, a specific inhibitor of macropinocytosis that blocks Na^+/H^+ exchange, on the infectivity of AHSV-4 was assessed. EIPA has been shown to specifically inhibit macropinocytosis without affecting other endocytic pathways, including clathrin-mediated endocytosis (West et al., 1989; Meier et al., 2002; Koivusalo et al., 2010). Consistent with this activity, EIPA (100 µM) caused a significant reduction (>99%) in the uptake of dextran, a marker for macropinocytosis, but did not inhibit the uptake of transferrin (at least 200 cells counted in each of two independent experiments) (Fig. 7A). In pre-treated BSR cells infected with AHSV-4, marked inhibition of virus infection was obtained in the presence of EIPA. Indeed, counting of infected cells revealed that AHSV-4 infection was inhibited by 87% (Figs. 7B and 7C). Treatment of BSR cells with different concentrations of EIPA decreased the progeny virus titre of AHSV-4 and VP5 protein expression in a dose-dependent manner. At the highest concentration tested, progeny virus production (2×10^3 pfu/ml) was reduced by 2 log units compared to the infected, mock-treated control cells (1.8×10^5 pfu/ml) and expression of VP5 was not detected (Figs. 7C and 7D).

To further explore the role of macropinocytosis in AHSV-4 entry, BSR cells were pre-treated with an inhibitor specific for Rac1, CAS 1177865-17-6, as well as with the PAK1-specific inhibitor IPA-3 and the PI3K-specific inhibitor Wortmannin. Rac1, PAK1 and PI3K are each involved in the regulation of macropinocytosis (Amyere et al., 2000; West et al., 2000; Mercer and Helenius, 2009). The functionality of the inhibitors was first verified by their inhibitory effect on dextran uptake (Fig. 8A). Infection of BSR cells by AHSV-4 was reduced by 36% in cells treated with Rac1 inhibitor (50 μM), by 70% in cells treated with IPA-3 (10 μM) and by 63% in cells treated with Wortmannin (100 nM) (Figs. 8B and 8C). The inhibitory effect of these treatments on AHSV-4 infection was also investigated in BSR cells treated with different concentrations of the respective inhibitors. The results indicated a dosage dependent reduction in both progeny virus production and VP5 protein expression (Figs. 8D and 8E).

Taken together, the above findings are consistent with the notion that macropinocytosis is required for AHSV-4 entry into BSR cells.

Discussion

Endocytosis offers an effective way for viruses to cross the physical barrier imposed by the plasma membrane and to traverse the underlying cortical matrix. Clathrin-mediated endocytosis is generally used by viruses that require a low pH-step during the early stages of infection to result in productive infection, whereas the lipid raft/caveolae-based route is typically used by acid-independent viruses (Klasse et al., 1998; Siazkarski and Whittaker, 2002; Marsh and Helenius, 2006; Mercer et al., 2010b). In recent years, macropinocytosis has generated much interest since it is used by some viruses from diverse families as a means to gain entry into cells (Mercer and Helenius, 2009). In this study, entry of AHSV-4 into BSR cells was investigated by examining the contribution of these endocytic pathways to virus cellular uptake.

It has been reported previously that infection of cells by BTV-10 is acid-activated and can be inhibited by raising endosomal pH (Forzan et al., 2007). In accordance with this observation, Forzan et al. (2007) concluded that BTV-10 infection of Vero and HeLa cells is mediated by clathrin-mediated endocytosis with capsid disassembly and membrane penetration occurring from within early endosomes. In this study, evidence was obtained that active endosomal

acidification is required for AHSV-4 infection of BSR cells. However, we found that clathrin-mediated endocytosis is not the major entry pathway used by AHSV-4 to infect BSR cells. Cell entry and infection was not inhibited by treatment of BSR cells with CPZ or a hypertonic medium, even though the respective treatments were able to block uptake of transferrin into cells, thus demonstrating that the treatments were effective for blocking clathrin-mediated endocytosis.

Our results suggested that during entry into BSR cells, AHSV-4 is delivered to acidic components via a clathrin-independent pathway. Since it has been shown that cargo internalized via caveolae can be delivered to acidic early endosomes (Pelkmans et al., 2004; Engel et al., 2011), we next considered the involvement of lipid raft/caveolae-based endocytosis in virus uptake. However, AHSV-4 entry and infection of BSR cells was not inhibited in cholesterol-depleted cells by treatment with MβCB or in cells subjected to cholesterol disorganization by treatment with nystatin, which is a sterol-reducing drug that sequesters cholesterol. Thus, the ability of AHSV-4 to productively infect BSR cells is not dependent on cholesterol and therefore virus uptake appears to be independent of lipid raft/caveolae-mediated entry mechanisms. This result is in concordance with previous studies (Forzan et al., 2007; Gold et al., 2010) showing that the presence of cholesterol in cellular membranes is not required for BTV infection in different cell lines (HeLa, Vero and BHK-21). Different non-clathrin/non-caveolae virus entry pathways are known to originate from raft areas in mammalian cells (Kirkham and Parton, 2005; Mayor and Pagano, 2007; Doherty and McMahon, 2009). Amongst these, the GEEC (GPI-anchored protein-enriched Endocytic Compartments) endocytic pathway leads to acidic endosomes (Kalia et al., 2006). This clathrin- and caveolae-independent pathway is, however, highly sensitive to cholesterol depletion (Sabharanjak et al., 2002) and is therefore unlikely to mediate AHSV-4 uptake.

The above results suggested that AHSV-4 enters cells through a route that is different from clathrin-mediated and lipid raft/caveolin-mediated endocytic pathways. Examination of thin sections of infected cells by transmission electron microscopy indicated that AHSV-4 causes a rearrangement of the BSR cells, leading to the formation of membrane protrusions that engulf the virus, which were then internalized into the cell cytoplasm within large endosomes corresponding to macropinosomes. These observations provided an initial indication that macropinocytosis could be involved in AHSV-4 entry of BSR cells. Moreover, Gold et al. (2010) reported that BTV-1 may enter BHK-21 cells by a macropinocytosis-like mechanism.

Taking this into consideration together with our results, we determined the effect of a number of inhibitors known to disrupt viral entry by macropinocytosis. In particular EIPA, an inhibitor of the Na^+/H^+ exchanger that specifically inhibits macropinocytosis (West et al., 1989; Koivusalo et al., 2010), and the actin depolymerizing agent cytochalasin D had an inhibitory effect on AHSV-4 entry and infection. Inhibition of Rac1, PI3K and PAK1, which have been implicated in the control of macropinocytosis (Mercer and Helenius, 2009), also had an inhibitory effect on virus infection. In contrast to inhibition of Pak1 and PI3K, inhibition of Rac1 caused a more moderate reduction in AHSV-4 infectivity. Considering that macropinocytosis is induced via a multi-branched signaling cascade (Mercer and Helenius, 2009; Kerr and Teasdale, 2009), redundancy could provide an explanation as to why inhibition of Rac1 was not total. For example, Cdc42, in addition to Rac1, is also responsible for the induction of actin filament accumulation at the plasma membrane that leads to membrane ruffling and macropinocytosis (Ridley et al., 1992; Garrett et al., 2000). Furthermore, Rac1 and Cdc42 are responsible for activating a series of kinases (Pak1, PI3K, PKC, PLCγ and PLC-A2) that regulate macropinocytosis by acting to promote membrane ruffling or by playing a role in macropinosome closure (Araki et al., 1996; Amyere et al., 2000; Liberali et al., 2008; Mercer and Helenius, 2009). Nevertheless, taken altogether, the results obtained provide compelling evidence that the endocytic pathway that AHSV-4 uses for entry and infection of BSR cells is macropinocytosis.

Although the trafficking pathway was not investigated in this study, it is noteworthy that, during maturation, macropinosomes undergo acidification (Yamauchi and Helenius, 2013; Cossart and Helenius, 2014) and/or can undergo heterotypic fusion with other vesicles of the classical endolysosomal pathway thereby successively transferring the cargo to more acidic compartments such as the early and late endosomes or lysosomes (Racoosin and Swanson, 1993; Pernet et al., 2009; Saeed et al., 2010; Rossman et al., 2012). Each of these vesicles/compartments can therefore provide the necessary cues to promote disassembly of the AHSV outer capsid proteins and acid-induced membrane penetration to release the transcriptionally active core particle into the cell cytoplasm. However, further investigations are required to determine which of these vesicles/compartments is the site of infection.

Constitutive macropinocytosis occurs in specific cell types such as dendritic cells and macrophages; however, in epithelial cells and fibroblasts, it is initiated in response to growth factor stimulation (Klasse et al., 1998) or expression of ruffling kinases (Amyere et al., 2000;

Dharmawardhane et al., 2000). Our electron microscopy studies of BSR cells incubated with AHSV-4 indicated that not only does AHSV-4 induce cell ruffling, but the virus is internalized along with HRP (a fluid phase marker) and does itself induce fluid-phase uptake. The data thus suggest that AHSV-4 virions are capable of triggering macropinocytosis. Viruses use different mechanisms to induce macropinocytosis. Vaccinia virus has been shown to trigger macropinocytosis by mimicking apoptotic bodies (Mercer and Helenius, 2008). In contrast, Coxsackie virus and adenovirus activate macropinocytosis by binding to the cell surface proteins occludin and integrin α_V, respectively (Meier et al., 2002; Coyne et al., 2007), whereas activation of Ax1 (a cell receptor tyrosine kinase) specifically enhances the macropinocytic uptake of Ebola virus (Hunt et al., 2011). The mechanism by which AHSV-4 triggers macropinocytosis in BSR cells is currently unknown, but likely involves interaction between its surface protein (VP2) and cellular receptors. Considering that AHSV infects and replicates in a wide range of cells (Meiring et al., 2009; Clift and Penrith, 2010; Stassen et al., 2012), it is plausible that its entry into cells is mediated by the binding of VP2 to a widely expressed and highly conserved receptor, or by VP2 binding to different host receptors. To date, receptors or co-receptors that may promote binding and subsequent uptake of AHSV into cells have not been identified.

Interestingly, the results of this study indicated that AHSV-4 uptake was inhibited by the dynamin inhibitor, dynasore, suggesting that the mechanism used by AHSV-4 to enter BSR cells is dynamin dependent. Dynamin is a large GTPase that has been described as a mechanochemical enzyme needed for the release of internalized vesicles from the plasma membrane and as a regulatory molecule that recruits and activates effectors in its GTP-bound form (Henley et al., 1999; Orth et al., 2003; Harper et al., 2013). Although dynamin was previously thought to be specific for clathrin-mediated endocytosis, it has become increasingly clear that it is also required for caveolae-mediated endocytosis, and some clathrin- and caveolae-independent endocytic pathways including phagocytosis (Oh et al., 1998; Henley et al., 1998; Gold et al., 1999; Mettlen et al., 2009; Doherty and McMahon, 2009). The involvement of dynamin in macropinocytosis is not clear and studies investigating its role have reported conflicting results (Mercer et al., 2010a; Kalin et al., 2010; Mulherkar et al., 2011; Saeed et al., 2010; Sánchez et al., 2012). In addition to its property of severing membranes, dynamin has been implicated in actin-membrane processes, such as the formation of podosomes, membrane extension and protrusion during lamellipodial advance, as well as vesicle trafficking (Ochoa et al., 2000; Orth et al., 2002; Ferguson and De Camilli,

2012). Thus, the dynamin dependence of AHSV-4 entry might not only be the result of its participation in the endocytosis pathway *per se*, but it might also be required for the trafficking of vesicles within the cell during the later stages of the infection cycle.

In conclusion, the results described in this study indicate that AHSV-4 utilized a dynamin-dependent macropinocytosis pathway as the primary means of entry into BSR cells. Furthermore, infection by AHSV-4 is activated and required a low endosomal pH for presumably disassembly of the outer capsid and membrane penetration to release transcriptionally active core particles into the cell cytoplasm, thus resulting in productive infection. Further studies will be required to investigate whether results obtained with BSR cells can be extrapolated to the natural target cells of AHSV, as well as the relevance of this pathway to pathogenesis in the animal host.

Materials and Methods

Cells and viruses

BSR cells (a clone of Baby Hamster Kidney-21 cells) were cultured at 37°C and 5% CO_2 in Eagle's minimum essential medium (EMEM) supplemented with Earle's balanced salt solution (EBSS), 2 mM L-glutamine, 5% (v/v) foetal bovine serum (FBS), 1% (v/v) non-essential amino acids (NEAA), and antibiotics (10 000 U/ml of penicillin, 10 000 µg/ml of streptomycin, 25 µg/ml of amphotericin B) (Hyclone).
AHSV serotype 4 (AHSV-4) was used in all experiments. Virus was grown on BSR cells and sucrose gradient-purified according to the method described by Huismans et al. (1987). Purified virus was stored at 4°C and the infectious titre was determined by plaque assay on BSR cells.

Antibodies

Polyclonal antibodies specific to the NS2 and VP5 proteins of AHSV-4 were generated by immunizing rabbits with the following peptides: NS2 protein amino acids (aa) 202 to 115 (CLDEAGPSRTPRKLS) and VP5 protein aa 133 to 146 (IVKGEVDAEKLEGNC). Peptide synthesis and antibody production was carried out by GenScript Corp. The specificity of these antibodies was verified by immunoblotting against AHSV-4-infected BSR cell lysates

using uninfected cells as a negative control. In the case of the anti-NS2 antibody, lack of cross-reactivity with uninfected BSR cells was also verified by confocal microscopy. The expression of cellular actin was monitored with a goat anti-β-actin antibody (Santa Cruz Biotechnology, Inc.). As secondary antibody, Protein-A conjugated to horseradish peroxidase (Sigma-Aldrich) was used for immunoblotting and fluorescein isothiocyanate (FITC)-conjugated goat anti-rabbit IgG (Sigma-Aldrich) was used for confocal microscopy. Primary antibodies were used at dilutions of 1:100 and secondary antibodies at dilutions of 1:400.

Pharmacological reagents

Alexa-Fluor-labelled transferrin, dextran and phalloidin were obtained from Invitrogen. All pharmacological inhibitors were purchased from Sigma-Aldrich, except for the Rac1 inhibitor (CAS 1177865-17-6) that was obtained from Calbiochem. Stock solutions of transferrin, dextran and methyl-β-cyclodextrin were made in EMEM, and stock solutions of the other inhibitors were prepared either in sterile water or DMSO, as per manufacturer's recommendation. Where applicable, an equivalent dilution of sterile water or DMSO was included in the mock treatment. The toxicity of the inhibitors to BSR cells was determined using the CellTiter 96 AQueous One Solution Cell Proliferation Assay (Promega) according to the manufacturer's protocol. The highest concentrations of each reagent that did not affect cell viability (>97%; Supplementary Table S1) was used in subsequent experiments, thus ensuring that the reduction in viral entry was due to a specific action on the entry pathway and not a general effect on cell viability.

Inhibitor treatment

BSR cell monolayers were grown on sterile glass coverslips in 24-well tissue culture plates. After washing in serum-free medium, the cells were pre-treated with inhibitors at the indicated concentrations for 30 min at 37°C. AHSV-4 was then added, using a MOI of 1 pfu/cell. After incubation at 4°C for 1 h to allow virus binding, the unbound virus was removed by three washes with incomplete EMEM and fresh medium containing the inhibitor was added to the cells, followed by incubation at 37°C. For pre-treatment of BSR cells with the lysosomotrophic drugs ammonium chloride (AC) at 25 mM and chloroquine (CQ) at 200 µM, a similar protocol was used except that the drugs remained present only during the virus binding step. These drugs were also added to BSR cells either coincident with the start of

infection (i.e. on shifting the temperature to 37°C) or at different times after infection was initiated. All experiments were ended at 24 h post-infection by the addition of 4% (w/v) paraformaldehyde (PFM) for 30 min. Virus-infected cells were identified using confocal microscopy and the anti-NS2 antibody, as described below.

Immunofluorescence confocal microscopy

After cell fixation with PFM, the cells were washed twice with PBS (pH 7.4) and permeabilized with 0.2% (v/v) Triton X-100 in PBS for 20 min. Non-specific binding sites were blocked in 5% blocking buffer (5% [w/v] milk powder in PBS) for 30 min after which the cells were incubated with the anti-NS2 antibody (diluted in 1% blocking buffer) for 1 h. The cells were then washed with wash buffer (0.5% [v/v] Tween-20 in PBS) and incubated with FITC-conjugated secondary antibody for 1 h. Cells were washed twice with wash buffer and once with PBS after which the coverslips were then mounted onto glass slides using ProLong Gold antifade reagent with DAPI (Life Technologies). The slides were viewed with a Zeiss LSM S10 Meta confocal microscope. For quantification of the percentage of infected cells in the presence of chemical inhibitors, cells with cytoplasmic labelling for AHSV-4 NS2 were scored as positive. To this end, a minimum of 15 random fields of view were observed, with a minimum of 200 cells quantified per inhibitor experiment. Two independent experiments were performed for each inhibitor tested. The level of infection of inhibitor-treated cells was normalized to the level of infection of the mock-treated control and the data are expressed as means ± SD. Representative images were captured with a Zeiss Axiovert Series 5 digital camera.

Virus titration

Treated and mock-treated cells infected with AHSV-4 were harvested at 24 h post-infection, washed, lysed and the relative virus titres determined by plaque assays on BSR cells. Confluent cell monolayers in 6-well tissue culture plates were incubated at 37°C for 1 h with diluted virus. The cells were then rinsed twice with incomplete EMEM to remove unadsorbed virus and overlaid with 1 ml of 0.5% (w/v) agarose in complete EMEM. Plaques were visualized after an incubation period of three days by staining with 0.1% (w/v) MTT (3-(4,5-dimethylthiazol-2-yl)-2,5-diphenyltetrazolium bromide).

Immunoblotting

Treated and mock-treated cells infected with AHSV-4 were harvested at 24 h post-infection, washed and suspended in PBS prior to mixing with an equal volume of 2 × Protein Solvent Buffer (PSB: 125 mM Tris-HCl [pH 6.8]; 4% [w/v] SDS; 20% [v/v] glycerol; 10% [v/v] 2-mercaptoethanol; 0.002% [w/v] bromophenol blue). Proteins were resolved by 10% (w/v) SDS-polyacrylamide gel electrophoresis (SDS-PAGE) and transferred to Hybond-C nitrocellulose membrane (Amersham Pharmacia Biotech AB) with a semi-dry electro-blotter (Hoefer) using standard protocols (Sambrook and Russell, 2001). The membrane was incubated with the appropriate primary antibody and horseradish peroxidase-conjugated Protein A was used for detection. Bands corresponding to VP5 and β-actin were densitometrically quantified, and data were normalized to control values (mock-treated virus-infected cells) with the TotalLab Quant v.1.0 software package (TotalLab Ltd.).

Transferrin and dextran uptake assays

The ability of BSR cells to internalize through the clathrin-mediated pathway was determined by observing transferrin uptake by confocal microscopy. Cells were serum-starved for 30 min prior to the addition of Alexa-568-labelled transferrin (25 µg/ml) in EMEM at 37°C for 15 min. Treated cells were washed once with PBS and then acid washed (0.1 M NaCl-0.1 M glycine, pH 3.0) to remove uninternalized transferrin (Hernaez and Alonso, 2010). For quantification of transferrin uptake, cells with cytoplasmic labelling for Alexa-568 transferrin were scored as positive. A similar protocol was followed to determine the ability of BSR cells to internalize through macropinocytosis, except that Alexa-568-labelled dextran (1 mg/ml) was added to serum-starved BSR cells, followed by incubation at 37°C for 30 min. The treated cells were then washed once with PBS and surface-bound dextran was washed off in 0.1 M NaOAc-0.05 M NaCl (pH 5.5) (Hernaez and Alonso, 2010).

Labelling of cellular cholesterol and actin filaments

Cellular cholesterol was labelled with filipin (125 µg/ml) for 15 min at room temperature and visualized immediately by confocal microscopy at 430 nm (Keller and Simons, 1998). To label for actin filaments, BSR cells were fixed and permeabilized, as described above, and

incubated with Alexa-568-labelled phalloidin for 10 min at room temperature. Actin filaments were visualized by confocal microscopy at 543 nm.

Transmission electron microscopy

BSR cells were grown inside 200-µm cellulose microcapillary tubes (LEICA Supplies) and infected with AHSV-4 at a MOI of 10 pfu/ml, using the inherent capillary action of the tubes by placing the end of the tube into the virus inoculum (Venter et al., 2012). Following incubation for 15, 30 and 60 min at 37°C, the microcapillary tubes were subjected to high pressure freezing. Freeze substitution was subsequently performed with a mixture of acetone containing 1% (v/v) osmium tetraoxide and 1% (v/v) distilled water (Venter et al., 2012). The tubes were embedded in Embed 812 resin, and ultrathin sections were stained in 5% (v/v) uranyl acetate and counterstained in 3% (v/v) Reynolds' lead citrate. The preparations were examined and photographed in a JOEL JEM 2100F transmission electron microscope.

Intracellular horseradish peroxidase (HRP) labelling experiments

For HRP labelling experiments, BSR cells grown within cellulose microcapillary tubes were infected with AHSV-4 at a MOI of 10 pfu/ml in the presence of 10 mg/ml HRP (Sigma, Type II). HRP was subsequently detected with 0.1% (w/v) diaminobenzidine (Sigma) for 10 min, followed by another 20 min in 0.1% (w/v) diaminobenzidine supplemented with 0.1% (v/v) H_2O_2 (Laakkonen et al., 2009). The cells were then washed with PBS supplemented with 0.5% (w/v) BSA and processed for transmission electron microscopy, as described above.

HRP uptake assay

HRP (2 mg/ml HRP in EMEM containing 1% [v/v] FBS) was added to BSR cell monolayers in the absence or presence of AHSV-4 (MOI of 10 pfu/cell). Following internalization at 37°C for 1 h, the cells were placed on ice and washed extensively with PBS supplemented with 0.5% (w/v) BSA to remove plasma membrane-bound HRP. The cells were harvested, suspended in PBS containing 1% (v/v) Triton X-100 and incubated on ice for 30 min. Cell debris was subsequently removed by centrifugation at 15 000 × g for 5 min. The protein concentration in the supernatant was determined with the Quick Start Bradford Protein Assay kit (BioRad). The HRP enzymatic activity was measured as described previously (Gruenberg

et al., 1989). For this purpose, 0.342 mM diaminobenzidine and 0.003% (v/v) H_2O_2 were used as substrates in 0.5 M Na-phosphate buffer (pH 5.0) containing 0.3% (v/v) Triton X-100, and HRP activity was measured at 460 nm in an Eppendorf Biophotometer Plus spectrophotometer.

Acknowledgments

This work was supported by the University of Pretoria's Institutional Research Theme Programme (Grant AOU999) and the National Research Foundation, South Africa (Grant 81068). Graduate bursary support was received from the National Research Foundation and University of Pretoria. We thank Mr. F. Wege for technical support with cell culture, and Mr. A. Hall and Miss A. Buys from the Microscopy and Microanalysis Unit at the University of Pretoria, as well as Dr. E. Venter for support with confocal microscopy and transmission electron microscopy.

References

Amyere, M., Payrastre, B., Krause, U., Van Der Smissen, P., Veithen, A., Courtoy, P.J., 2000. Constitutive macropinocytosis in oncogene-transformed fibroblasts depends on sequential permanent activation of phosphoinositide 3-kinase and phospholipase C. Mol. Biol. Cell 11, 3453-3467.

Araki, N., Johnson, M.T., Swanson, J.A., 1996. A role for phosphoinositide 3-kinase in the completion of macropinocytosis and phagocytosis by macrophages. J. Cell Biol. 135, 1249-1260.

Clift, S.J., Penrith, M.L., 2010. Tissue and cell tropism of African horse sickness virus demonstrated by immunoperoxidase labeling in natural and experimental infection in horses in South Africa. Vet. Pathol. 47, 690-697.

Cossart, P., Helenius, A., 2014. Endocytosis of viruses and bacteria. Cold Spring Harb. Perspect. Biol. 6, a016972.

Coyne, C.B., Shen, L., Turner, J.R., Bergelson, J.M., 2007. Coxsackievirus entry across epithelial tight junctions requires occludin and the small GTPases Rab34 and Rab5. Cell Host Microbe 2, 181-192.

de Vries, E., Tscherne, D.M., Wienholts, M.J., Cobos-Jimenez, V., Scholte, F., Garcia-Sastre, A., Rottier, P.J., de Haan, C.A., 2011. Dissection of the influenza A virus endocytic routes reveals macropinocytosis as an alternative entry pathway. PLoS Pathog. 7, e1001329.

Dharmawardhane, S., Schürmann, A., Sells, M.A., Chernoff, J., Schmid, S.L., Bokoch, G.M., 2000. Regulation of macropinocytosis by p21-activated kinase-1. Mol. Biol. Cell 11, 3341-3352.

Doherty, G.J., McMahon, H.T., 2009. Mechanisms of endocytosis. Annu. Rev. Biochem. 78, 857-902.

Engel, S., Heger, T., Mancini, R., Herzog, F., Kartenbeck, J., Hayer, A., Helenius, A., 2011. Role of endosomes in simian virus 40 entry and infection. J. Virol. 85, 4198-4211.

Ferguson, S.M., De Camilli, P., 2012. Dynamin, a membrane-remodelling GTPase. Nature Rev. Mol. Cell Biol. 13, 75-88.

Forzan, M., Marsh, M., Roy, P., 2007. Bluetongue virus entry into cells. J. Virol. 81, 4819-4827.

Garcin, P.O., Panté, N., 2015. The minute virus of mice exploits different endocytic pathways for cellular uptake. Virology 482, 157-166.

Garrett, W.S., Chen, L.M., Kroschewski, R., Ebersold, M., Turley, S., Trombetta, S., Galan, J.E., Mellman, I., 2000. Developmental control of endocytosis in dendritic cells by Cdc42. Cell 102, 325-334.

Gerondopoulos, A., Jackson, T., Monaghan, P., Doyle, N., Roberts, L.O., 2010. Murine norovirus-1 cell entry is mediated through a non-clathrin, non-caveolae, dynamin- and cholesterol-dependent pathway. J. Gen.Virol. 91, 1428-1438.

Goddette, D.W., Frieden, C., 1986. Actin polymerization. The mechanism of action of cytochalasin D. J. Biol. Chem. 261, 15974-15980.

Gold, E.S., Underhill, D.M., Morrissette, N.S., Guo, J., McNiven, M.A., Aderem, A., 1999. Dynamin-2 is required for phagocytosis in macrophages. J. Exp. Med. 190, 1849-1856.

Gold, S., Monaghan, P., Mertens, P., Jackson, T., 2010. A clathrin-independent macropinocytosis-like entry mechanism used by bluetongue virus-1 during infection of BHK cells. PLoS One 5, e11360.

Gruenberg, J., Griffiths, G., Howell, K.E., 1989. Characterization of the early endosome and putative endocytic carrier vesicles *in vivo* and with an assay of vesicle fusion *in vitro*. J. Cell Biol. 108, 1301-1316.

Hansen, S.H., Sandvig, K., van Deurs, B., 1993. Clathrin and HA2 adaptors: effects of potassium depletion, hypertonic medium, and cytosol acidification. J. Cell Biol. 121, 61-72.

Harper, C.B., Popoff, M.R., McCluskey, A., Robinson, P.J., Meunier, F.A., 2013. Targeting membrane trafficking in infection prophylaxis: dynamin inhibitors. Trends Cell Biol. 23, 90-101.

Hassan, S.H., Wirblich, C., Forzan, M., Roy, P., 2001. Expression and functional characterization of bluetongue virus VP5 protein: role in cellular permeabilization. J. Virol. 75, 8356-8367.

Hassan, S.S., Roy, P., 1999. Expression and functional characterization of bluetongue virus VP2 protein: role in cell entry. J. Virol. 73, 9832-9842.

Hayer, A., Stoeber, M., Ritz, D., Engel, S., Meyer, H.H., Helenius, A., 2010. Caveolin-1 is ubiquitinated and targeted to intralumenal vesicles in endolysosomes for degradation. J. Cell. Biol. 191, 615-629.

Helenius, A., Kartenbeck, J., Simons, K., Fries, E., 1980. On the entry of Semliki Forest virus into BHK-21 cells. J. Cell Biol. 84, 404-420.

Henley, J.R., Cao, H., McNiven, M.A., 1999. Participation of dynamin in the biogenesis of cytoplasmic vesicles. FASEB J. 13 Suppl. 2, S243-247.

Henley, J.R., Krueger, E.W., Oswald, B.J., McNiven, M.A., 1998. Dynamin-mediated internalization of caveolae. J. Cell Biol. 141, 85-99.

Hernaez, B., Alonso, C., 2010. Dynamin- and clathrin-dependent endocytosis in African swine fever virus entry. J. Virol. 84, 2100-2109.

Heuser, J.E., Anderson, R.G., 1989. Hypertonic media inhibit receptor-mediated endocytosis by blocking clathrin-coated pit formation. J. Cell Biol. 108, 389-400.

Hinshaw, J.E., 2000. Dynamin and its role in membrane fission. Annu. Rev. Cell. Dev. Biol. 16, 483-519.

Huang, W.R., Wang, Y.C., Chi, P.I., Wang, L., Wang, C.Y., Lin, C.H., Liu, H.J., 2011. Cell entry of avian reovirus follows a caveolin-1-mediated and dynamin-2-dependent endocytic pathway that requires activation of p38 mitogen-activated protein kinase (MAPK) and Src signaling pathways as well as microtubules and small GTPase Rab5 protein. J. Biol. Chem. 286, 30780-30794.

Huismans, H., van der Walt, N.T., Cloete, M., Erasmus, B.J., 1987. Isolation of a capsid protein of bluetongue virus that induces a protective immune response in sheep. Virology 157, 172-179.

Hunt, C.L., Kolokoltsov, A.A., Davey, R.A., Maury, W., 2011. The Tyro3 receptor kinase Axl enhances macropinocytosis of Zaire ebolavirus. J. Virol. 85, 334-347.

Kalia, M., Kumari, S., Chadda, R., Hill, M.M., Parton, R.G., Mayor, S., 2006. Arf6-independent GPI-anchored protein-enriched early endosomal compartments fuse with sorting

endosomes via a Rab5/phosphatidylinositol-39-kinase-dependent machinery. Mol. Biol. Cell 17, 3689-3704.

Kalin, S., Amstutz, B., Gastaldelli, M., Wolfrum, N., Boucke, K., Havenga, M., DiGennaro, F., Liska, N., Hemmi, S., Greber, U.F., 2010. Macropinocytotic uptake and infection of human epithelial cells with species B2 adenovirus type 35. J. Virol. 84, 5336-5350.

Kar, A.K., Bhattacharya, B., Roy, P., 2007. Bluetongue virus RNA binding protein NS2 is a modulator of viral replication and assembly. BMC Mol. Biol. 8, 4.

Kartenbeck, J., Stukenbrok, H., Helenius, A., 1989. Endocytosis of simian virus 40 into the endoplasmic reticulum. J. Cell Biol. 109, 2721-2729.

Keller, P., Simons, K., 1998. Cholesterol is required for surface transport of influenza virus hemagglutinin. J. Cell Biol. 140, 1357-1367.

Kerr, M.C., Teasdale, R.D., 2009. Defining macropinocytosis. Traffic 10, 364-371.

Khan, A.G., Pickl-Herk, A., Gajdzik, L., Marlovits, T.C., Fuchs, R., Blaas, D., 2011. Entry of a heparin sulphate-binding HRV8 variant strictly depends on dynamin but not on clathrin, caveolin, and flotillin. Virology 412, 55-67.

Kirkham, M., Parton, R.G., 2005. Clathrin-independent endocytosis: New insights into caveolae and non-caveolar lipid raft carriers. Biochim. Biophys. Acta 1745, 273-286.

Klasse, P.J., Bron, R., Marsh, M., 1998. Mechanisms of enveloped virus entry into animal cells. Adv. Drug Deliv. Rev. 34, 65-91.

Koivusalo, M., Welch, C., Hayashi, H., Scott, C.C., Kim, M., Alexander, T., Touret, N., Hahn, K.M., Grinstein, S., 2010. Amiloride inhibits macropinocytosis by lowering submembraneous pH and preventing Rac1 and Cdc42 signaling. J. Cell Biol. 188, 547-563.

Laakkonen, J.P., Mäkelä, A.R., Kakkonen, E., Turkki, P., Kukkonen, S., Peränen, J., Ylä-Herttuala, S., Airenne, K.J., Oker-Blom, C., Vihinen-Ranta, M., Marjomäki, V., 2009.

Clathrin-independent entry of baculovirus triggers uptake of *E. coli* in non-phagocytic human cells. PLoS One 4, e5093.

Lajoie, P., Nabi, I.R., 2010. Lipid rafts, caveolae, and their endocytosis. Int. Rev. Cell. Mol. Biol. 282, 135-163.

Liberali, P., Kakkonen, E., Turacchio, G., Valente, C., Spaar, A., Perinetti, G., Böckmann, R.A., Corda, D., Colanzi, A., Marjomaki, V., Luini, A., 2008. The closure of Pak1-dependent macropinosomes requires the phosphorylation of CtBP1/BARS. EMBO J. 27, 970-981.

Macia, E., Ehrlich, M., Massol, R., Boucrot, E., Brunner, C., Kirchhausen, T., 2006. Dynasore, a cell permeable inhibitor of dynamin. Dev. Cell 10, 839-850.

Manole, V., Laurinmäki, P., van Wyngaardt, W., Potgieter, C.A., Wright, I.M., Venter, G.J., van Dijk, A.A., Sewell, B.T., Butcher, S.J., 2012. Structural insight into African horsesickness virus infection. J. Virol. 86, 7858-7866.

Marsh, M., Helenius, A., 2006. Virus entry: open sesame. Cell 124, 729-740.

Mayor, S., Pagano, R.E., 2007. Pathways of clathrin-independent endocytosis. Nature Rev. Mol. Cell Biol. 8, 603-612.

McMahon, H.T., Boucrot, E., 2011. Molecular mechanism and physiological functions of clathrin-mediated endocytosis. Nature Rev. Mol. Cell Biol. 12, 517-533.

Meier, O., Boucke, K., Hammer, S.V., Keller, S., Stidwill, R.P., Hemmi, S., Greber, U.F., 2002. Adenovirus triggers macropinocytosis and endosomal leakage together with its clathrin-mediated uptake. J. Cell Biol. 158, 1119-1131.

Meiring, T.L., Huismans, H., Van Staden, V., 2009. Genome segment reassortment identifies non-structural protein NS3 as a key protein in African horsesickness virus release and alteration of membrane permeability. Arch. Virol. 154, 263-271.

Mercer, J., Helenius, A., 2008. Vaccinia virus uses macropinocytosis and apoptotic mimicry to enter host cells. Science 320, 531-535.

Mercer, J., Helenius, A., 2009. Virus entry by macropinocytosis. Nature Cell Biol. 11, 510-520.

Mercer, J., Helenius, A., 2012. Gulping rather than sipping: macropinocytosis as a way of virus entry. Curr. Opin. Microbiol. 15, 1-10.

Mercer, J., Knébel, S., Schmidt, F.I., Crouse, J., Burkard, C., Helenius, A., 2010a. Vaccinia virus strains use different forms of macropinocytosis for host-cell entry. Proc. Natl. Acad. Sci. USA 107, 9346-9351.

Mercer, J., Schelhaas, M., Helenius, A., 2010b. Virus entry by endocytosis. Annu. Rev. Biochem. 79, 803-833.

Mettlen, M., Pucadyil, T., Ramachandran, R., Schmid, S.L., 2009. Dissecting dynamin's role in clathrin-mediated endocytosis. Biochem. Soc. Trans. 37, 1022-1026.

Moriyama, T., Marquez, J.P., Wakatsuki, T., Sorokin, A., 2007. Caveolar endocytosis is critical for BK virus infection of human renal proximal tubular epithelial cells. J. Virol. 81, 8552-8562.

Mulherkar, N., Raaben, M., de la Torre, J.C., Whelan, S.P., Chandran, K., 2011. The Ebola virus glycoprotein mediates entry via a non-classical dynamin-dependent macropinocytic pathway. Virology 419, 72-83.

Nonnenmacher, M., Weber, T., 2011. Adeno-associated virus 2 infection requires endocytosis through the CLIC/GEEC pathway. Cell Host Microbe 10, 563-576.

O'Donnell, V., LaRocco, M., Baxt, B., 2008. Heparan sulfate-binding foot-and-mouth disease virus enter cells via caveolae-mediated endocytosis. J. Virol. 82, 9075-9085.

Ochoa, G.C., Slepnev, V.I., Neff, L., Ringstad, N., Takei, K., Daniell, L., Kim, W., Cao, H., McNiven, M., Baron, R., De Camilli, P., 2000. A functional link between dynamin and the actin cytoskeleton at podosomes. J. Cell Biol. 150, 377-389.

Oh, P., McIntosh, D.P., Schnitzer, J.E., Losty, P.D., 1998. Dynamin at the neck of caveolae mediates their budding to form transport vesicles by GTP-driven fission from the plasma membrane of endothelium. J. Cell Biol. 141, 101-114.

Orth, J.D., Krueger, E.W., Cao, H., McNiven, M.A., 2002. The large GTPase dynamin regulates actin comet formation and movement in living cells. Proc. Natl. Acad. Sci. USA 99, 167-172.

Orth, J.D., McNiven, M.A., 2003. Dynamin at the actin-membrane interface. Curr. Opin. Cell Biol. 15, 31-39.

Palacios, M., Padron, J., Glaria, L., Rojas, A., Delgado, R., Knowles, R., Moncada, S., 1993. Chlorpromazine inhibits both the constitutive nitric oxide synthase and the induction of nitric oxide synthase after LPS challenge. Biochem. Biophys. Res. Commun. 196, 280-286.

Parton, R.G., 2003. Caveolae - from ultrastructure to molecular mechanisms. Nature Rev. Mol. Cell Biol. 4, 162-167.

Parton, R.G., Simons, K., 2007. The multiple faces of caveolae. Nature Rev. Mol. Cell Biol. 8, 185-194.

Pelkmans, L., Burli, T., Zerial, M., Helenius, A., 2004. Caveolin-stabilized membrane domains as multifunctional transport and sorting devices in endocytic membrane traffic. Cell 118, 767-780.

Pernet, O., Pohl, C., Ainouze, M., Kweder, H., Buckland, R., 2009. Nipah virus entry can occur by macropinocytosis. Virology 395, 298-311.

Piccinotti, S., Kichhausen, T., Whelan, S.P.J., 2013. Uptake of rabies virus into epithelial cells by clathrin-mediated endocytosis depends on actin. J. Virol. 87, 11637-11647.

Racoosin, E.L., Swanson, J.A., 1993. Macropinosome maturation and fusion with tubular lysosomes in macrophages. J. Cell. Biol. 121, 1011-1020.

Ridley, A.J., Paterson, H.F., Johnston, C.L., Diekmann, D., Hall, A., 1992. The small GTP-binding protein Rac regulates growth factor-induced membrane ruffling. Cell 70, 401-410.

Rossman, J.S., Leser, G.P., Lamba, R.A., 2012. Filamentous influenza virus enters cells via macropinocytosis. J. Virol. 86, 10950-10960.

Rothberg, K.G., Heuser, J.E., Donzell, W.C., Ying, Y.S., Glenney, J.R., Anderson, R.G., 1992. Caveolin, a protein component of caveolae membrane coats. Cell 68, 673-682.

Sabharanjak, S., Sharma, P., Parton, R.G., Mayor, S., 2002. GPI-anchored proteins are delivered to recycling endosomes via a distinct Cdc42-regulated, clathrin-independent pinocytic pathway. Dev. Cell 2, 411-423.

Saeed, M.F., Kolokoltsov, A.A., Albrecht, T., Davey, R.A., 2010. Cellular entry of Ebola virus involves uptake by a macropinocytosis-like mechanism and subsequent trafficking through early and late endosomes. PLoS Pathog. 6, e1001110.

Sambrook, J., Russell, D.W., 2001. Molecular Cloning, A Laboratory Manual, 3rd Ed., Cold Spring Harbour Laboratory Press, New York, USA.

Sánchez, E.G., Quintas, A., Pérez-Núñez, D., Nogal, M., Barroso, S., Carrascosa, Á.L., Revilla, Y., 2012. African swine fever virus uses macropinocytosis to enter host cells. PLoS Pathog. 8, e1002754.

Schliwa, M., 1982. Action of cytochalasin D on cytoskeletal networks. J. Cell Biol. 92, 79-91.

Sieczkarski, S.B., Whittaker, G.R., 2002. Dissecting virus entry via endocytosis. J. Gen. Virol. 83, 1535-1545.

Smart, E.J., Anderson, R.G.W., 2002. Alterations in membrane cholesterol that affect structure and function of caveolae. Methods Enzymol. 353, 131-139.

Stassen, L., Huismans, H., Theron, J., 2011. Membrane permeabilization of the African horse sickness virus VP5 protein is mediated by two N-terminal amphipathic α-helices. Arch. Virol. 156, 711-715.

Stassen, L., Huismans, H., Theron, J., 2012. African horse sickness virus induces apoptosis in cultured mammalian cells. Virus Res. 163, 385-389.

Stassen, L., Vermaak, E., Theron, J., 2014. African horse sickness, an equine disease of emerging global significance. In: Horses: Breeding, health disorders and effects on performance and behavior. Adolfo Paz-Silva, María Sol Arias Vázquez, Rita Sánchez-Andrade Fernández (Eds), pp. 145-170, Nova Publishers, New York.

Sun, X., Yau, V.K., Briggs, B.J., Whittaker, G.R., 2005. Role of clathrin-mediated endocytosis during vesicular stomatitis virus entry into host cells. Virology 338, 53-60.

Swanson, J.A. (2008). Shaping cups into phagosomes and macropinosomes. Nature Rev. Mol. Cell Biol. 9, 639-649.

Uitenweerde, J.M., Theron, J., Stoltz, M.A., Huismans, H., 1995. The multimeric nonstructural NS2 protein of Bluetongue virus, African horsesickness virus, and Epizootic hemorrhagic disease virus differ in their single-stranded RNA-binding ability. Virology 209, 624-632.

Venter, E., van der Merwe, C.F., van Staden, V., 2012. Utilization of cellulose microcapillary tubes as a model system for culturing and viral infection of mammalian cells. Microsc. Res. and Tech. 75, 1452-1459.

Wang, L.H., Rothberg, K.G., Anderson, R.G., 1993. Mis-assembly of clathrin lattices on endosomes reveals a regulatory switch for coated pit formation. J. Cell Biol. 123, 1107-1117.

West, M.A., Bretscher, M.S., Watts, C., 1989. Distinct endocytotic pathways in epidermal growth factor-stimulated human carcinoma A431 cells. J. Cell Biol. 109, 2731-2739.

West, M.A., Prescott, A.R., Eskelinen, E-L., Ridley, A.J., Watts, C., 2000. Rac is required for constitutive macropinocytosis by dendritic cells but does not control its own down-regulation. Curr. Biol. 10, 839-848.

Yamauchi, Y., Helenius, A., 2013. Virus entry at a glance. J. Cell Sci. 126, 1289-1295.

Figure legends

Fig. 1. Endosomal acidification is required for AHSV-4 infection of BSR cells. (A) BSR cells were mock-treated or pre-treated with 25 mM ammonium chloride (AC) or 200 µM chloroquine (CQ) and then infected with AHSV-4 at a MOI of 1 pfu/ml. At 24 h post-infection, the cells were processed for confocal microscopy and infected cells were identified using an anti-NS2 antibody (shown in green). The cell nuclei are shown in blue. Scale bar = 10 µm. (B) In addition to the pre-treatment (PT) of BSR cells described above, AC or CQ was also added to cells coincident with the start of infection (time 0) or at different times post-infection (30 and 120 min). At the end of infection, the cells were processed for confocal microscopy and at least 200 cells per time point for each treatment were counted. The level of infection of the drug-treated cells was normalized to the levels of infection of the mock-treated cells. The results are presented as means ± SD of two independent experiments.

Fig. 2. Infection of BSR cells by AHSV-4 is not inhibited by drugs that affect clathrin-mediated endocytosis. (A) BSR cells were mock-treated or pre-treated with 10 µM chlorpromazine (CPZ) or 0.45 M sucrose and allowed to internalize Alexa-568-labelled transferrin for 15 min, and processed for confocal microscopy. Transferrin is shown in red and the cell nuclei are shown in blue. Scale bar = 10 µm. (B) BSR cells were mock-treated or pre-treated with 10 µM CPZ or 0.45 M sucrose, followed by infection with AHSV-4 at a MOI of 1 pfu/ml in the continued presence of the drugs. At 24 h post-infection, cells were processed for confocal microscopy and infected cells were identified using an anti-NS2 antibody (shown in green). The cell nuclei are shown in blue. Scale bar = 10 µm. (C) Cells were scored for infection by confocal microscopy counting of at least 200 cells for the mock- and drug-treated cells in each of two independent experiments. The level of infection of the drug-treated cells was normalized to the level of infection of the mock-treated cells. The results are presented as means ± SD. (D) Similar to above, BSR cells were pre-treated with different concentrations of CPZ or sucrose and subsequently infected with AHSV-4. After incubation, cell lysates were prepared and virus titres determined by plaque assay. The data are means ± SD from three independent experiments. (E) Viral protein synthesis was evaluated at different drug concentrations, as indicated in the figure, by immunoblot analysis with an anti-VP5 antibody. To verify that the same amount of protein was loaded in each lane, the blot was also stained with an anti-β-actin antibody. Quantification of the bands

corresponding to VP5 was corrected with β-actin data and then normalized to the value from control mock-treated cells infected with AHSV-4.

Fig. 3. Infection of BSR cells by AHSV-4 is not inhibited by disruption of cholesterol-dependent endocytic mechanisms. (A) BSR cells were mock-treated or pre-treated with 2 µg/ml methyl-β-cyclodextrin (MβCD), and then incubated with filipin and viewed by confocal microscopy. Blue fluorescence represents filipin binding to cholesterol. Scale bar = 10 µm. (B) BSR cells were mock-treated or pre-treated with 2 µg/ml MβCD or 80 µg/ml nystatin, followed by infection with AHSV-4 at a MOI of 1 pfu/ml in the continued presence of the drugs. At 24 h post-infection, cells were processed for confocal microscopy and infected cells were identified using an anti-NS2 antibody (shown in green). The cell nuclei are shown in blue. Scale bar = 10 µm. (C) The bar graph shows quantitation of data shown in (B). For this, green fluorescent cells were counted and normalized to the level of infection of the mock-treated cells. At least 200 cells for the mock- and drug-treated cells were counted in each of two independent experiments and the results are presented as means ± SD. (D) Virus titres were determined by plaque assay of samples prepared at 24 h post-infection from BSR cells infected with AHSV-4 in the presence of different concentrations of MβCD or nystatin. The experiments were repeated three times and the data are presented as means ± SD. (E) Immunoblotting of cells infected with AHSV-4 after treatment with different concentrations of the respective drugs using anti-VP5 and anti-β-actin antibodies. Quantification of the bands corresponding to VP5 was corrected with β-actin data and then normalized to the value from control cells infected with AHSV-4.

Fig. 4. AHSV-4 infection of BSR cells is sensitive to dynamin inhibition by dynasore. (A) BSR cells were mock-treated or pre-treated with 100 µM dynasore and allowed to internalize Alexa-568-labelled transferrin for 15 min, or Alexa-568-labelled dextran for 30 min, and processed for confocal microscopy. Transferrin and dextran are shown in red, and the cell nuclei are shown in blue. Scale bar = 10 µm. (B) BSR cells were mock-treated or pre-treated with dynasore (100 µM) and then infected with AHSV-4 at a MOI of 1 pfu/ml in the continued presence of the drug. At 24 h post-infection, cells were processed for confocal microscopy and infected cells were identified using an anti-NS2 antibody (shown in green). The cell nuclei are shown in blue. Scale bar = 10 µm. (C) Cells were scored for infection by confocal microscopy counting of at least 200 cells for the mock- and drug-treated cells in each of two independent experiments. The level of infection of the drug-treated cells was

normalized to the level of infection of the mock-treated cells. The results are presented as means ± SD. (D) BSR cells were pre-treated with different concentrations of dynasore and then infected with AHSV-4 (1 pfu/ml) in the presence of the drug. Following 24-h incubation, virus titrations were performed. The data are means ± SD from three independent experiments. (E) Immunoblot analysis of cell lysates prepared from BSR cells infected with AHSV-4 after treatment with different concentrations of dynasore. In addition to an anti-VP5 antibody, the immunoblot was also stained with an anti-β-actin antibody to verify equal sample loading. Quantification of the bands corresponding to VP5 was corrected with β-actin data and then normalized to the value from control mock-treated cells infected with AHSV-4.

Fig. 5. Induction of macropinocytosis by AHSV-4. (A-C) BSR cells were infected with AHSV-4 at a MOI of 10 pfu/ml for different time periods, fixed and processed for viewing by transmission electron microscopy. (A) AHSV-4 infection induced ruffling and virions attached next to cellular extensions. (B) Cup-like indentations formed at the cell surface and large cellular extensions embraced AHSV-4. (C) Large smooth-surfaced endocytic vesicles containing AHSV-4. (D) As controls, BSR cells were either mock-infected or treated with 100 µM EIPA and infected with AHSV-4 in the presence of the drug. No membrane ruffling was observed in the control cells. Scale bars = 100 nm, unless otherwise indicated. Arrows indicate AHSV-4 virions. (E) Virus infection was performed as described above for 1 h in the presence or absence of the fluid phase marker HRP. HRP-negative and -positive vesicles containing AHSV-4 are presented. Arrows indicate AHSV-4 virions and arrowheads indicate the HRP-diaminobenzidine reaction product. Scale bars = 100 nm. (F) BSR cells were incubated with HRP and with or without AHSV-4. After 1-h incubation at 37°C, the cells were washed and the amount of internalized HRP was determined and normalized to the cellular protein content. The results are shown as the means ± SD of three independent experiments.

Fig. 6. Infection of BSR cells by AHSV-4 is inhibited by actin disruption. (A) BSR cells were mock-treated or treated with 5 µg/ml cytochalasin D (CytD), after which the cells were fixed, permeabilized and the actin filaments stained with Alexa-568-labelled phalloidin for 10 min. Successful disruption of the actin filaments (exhibiting red fluorescence) was confirmed by confocal microscopy. The cell nuclei are shown in blue. Scale bar = 10 µm. (B) BSR cells were mock-treated or pre-treated with cytochalasin D, followed by infection with AHSV-4 at a MOI of 1 pfu/ml in the continued presence of the drug. At 24 h post-infection,

cells were processed for confocal microscopy and infected cells were identified using an anti-NS2 antibody (shown in green). The cell nuclei are shown in blue. Scale bar = 10 μm. (C) The infectivity of AHSV-4 in mock- and drug-treated cells was quantified by confocal microscopy counting of at least 200 cells per treatment. The level of infection of the drug-treated cells was then normalized to the level of infection of the mock-treated cells. The results are presented as the means ± SD from two independent experiments. (D) Similar to above, BSR cells were mock-treated or pre-treated with different concentrations of cytochalasin D and then infected with AHSV-4. Cells were harvested and lysed at 24 h post-infection, and virus titres were determined by plaque assays. The data are means ± SD from three independent experiments. (E) Inhibition of viral protein synthesis was analyzed by immunoblotting of infected cell lysates with an anti-VP5 antibody at 24 h post-infection. Increasing concentrations of cytochalasin D were used, and β-actin was detected as control of protein loading. Quantification of the bands corresponding to VP5 was corrected with β-actin data and then normalized to the value from control mock-treated cells infected with AHSV-4.

Fig. 7. AHSV-4 infection of BSR cells is inhibited by EIPA. (A) To confirm the activity of EIPA, BSR cells (mock-treated or pre-treated with 100 μM EIPA) were incubated with Alexa-568-labelled transferrin or dextran (both red). After incubation, the cells were processed for confocal microscopy and analyzed for uptake of each marker. The cell nuclei are shown in blue. Scale bar = 10 μm. (B) BSR cells were mock-treated or pre-treated with EIPA, followed by infection with AHSV-4 at a MOI of 1 pfu/ml in the continued presence of the inhibitor. At 24 h post-infection, cells were processed for confocal microscopy and infected cells were identified using an anti-NS2 antibody (shown in green). The cell nuclei are shown in blue. Scale bar = 10 μm. (C) The data shown in (B) was quantified through scoring of the cells for infection by confocal microscopy counting of at least 200 cells per treatment. The level of infection of the EIPA-treated cells was normalized to the levels of infection of the mock-treated cells. The result is presented as the means ± SD of two independent experiments. (D) BSR cells were incubated with different concentrations of EIPA and then infected with AHSV-4 as above. At 24 h post-infection, cell lysates were prepared and the virus titres determined by plaque assays. The data are means ± SD from three independent experiments. (E) The effect of increasing concentrations of EIPA on viral protein synthesis at 24 h post-infection was determined by immunoblotting with an anti-VP5 antibody, and β-actin was detected as control of protein loading. Quantification of the bands

corresponding to VP5 was corrected with β-actin data and then normalized to the value from control mock-treated cells infected with AHSV-4.

Fig. 8. AHSV-4 infection of BSR cells is sensitive to Rac1, PI3K and Pak1 inhibition. (A) BSR cells were mock-treated or pre-treated with 50 μM Rac1 inhibitor, 10 μM IPA-3 or 100 nM Wortmannin and allowed to internalize Alexa-568-labelled dextran for 30 min, and processed for confocal microscopy. Dextran is shown in red and the cell nuclei are shown in blue. Scale bar = 10 μm. (B) BSR cells were mock-treated or pre-treated with the respective inhibitors, followed by infection with AHSV-4 at a MOI of 1 pfu/ml in the continued presence of the inhibitors. At 24 h post-infection, cells were processed for confocal microscopy and infected cells were identified using an anti-NS2 antibody (shown in green). The cell nuclei are shown in blue. Scale bar = 10 μm. (C) The number of infected cells was determined by confocal microscopy counting of the number of green fluorescent cells. At least 200 cells for the mock- and inhibitor-treated cells were counted in each of two independent experiments. The level of infection of the inhibitor-treated cells was normalized to the levels of infection of the mock-treated cells. (D) Virus titres of samples prepared at 24 h post-infection from BSR cells infected with AHSV-4 in the presence of different concentrations of Rac1 inhibitor, IPA-3 or Wortmannin. The data are means ± SD from three independent experiments. (E) The effects of different concentrations of the Rac1 inhibitor, IPA-3 and Wortmannin on viral protein synthesis were analyzed by immunoblotting of infected cell extracts with an anti-VP5 antibody at 24 h post-infection. To verify equal sample loading, the blots were also stained with an anti-β-actin antibody. Quantification of the bands corresponding to VP5 was corrected with β-actin data and then normalized to the value from control mock-treated cells infected with AHSV-4.

A

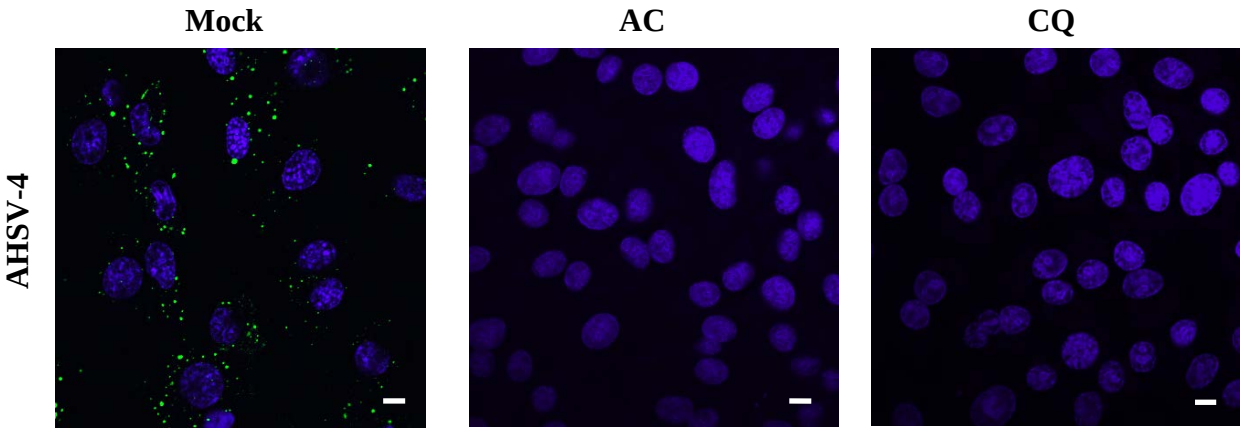
Mock
AC
CQ
AHSV-4

B

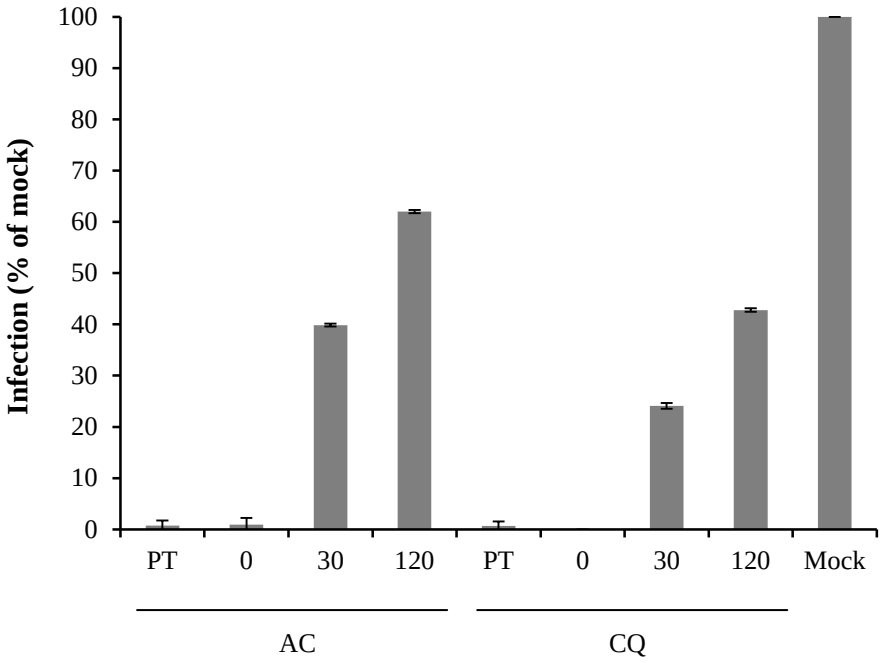
Infection (% of mock)
100
90
80
70
60
50
40
30
20
10
0
PT
0
30
120
PT
0
30
120
Mock
AC
CQ

Figure 1

A

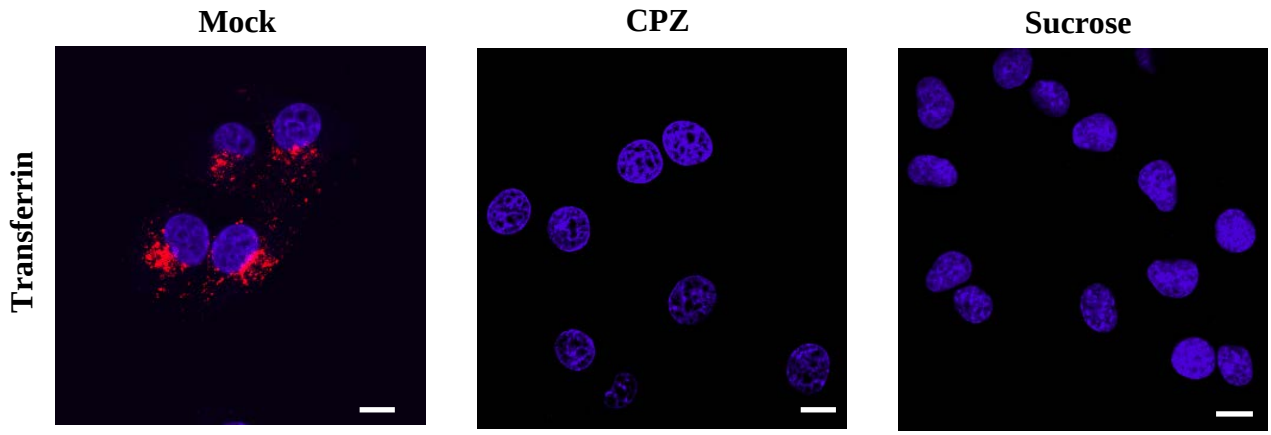
Mock
CPZ
Sucrose
Transferrin

B

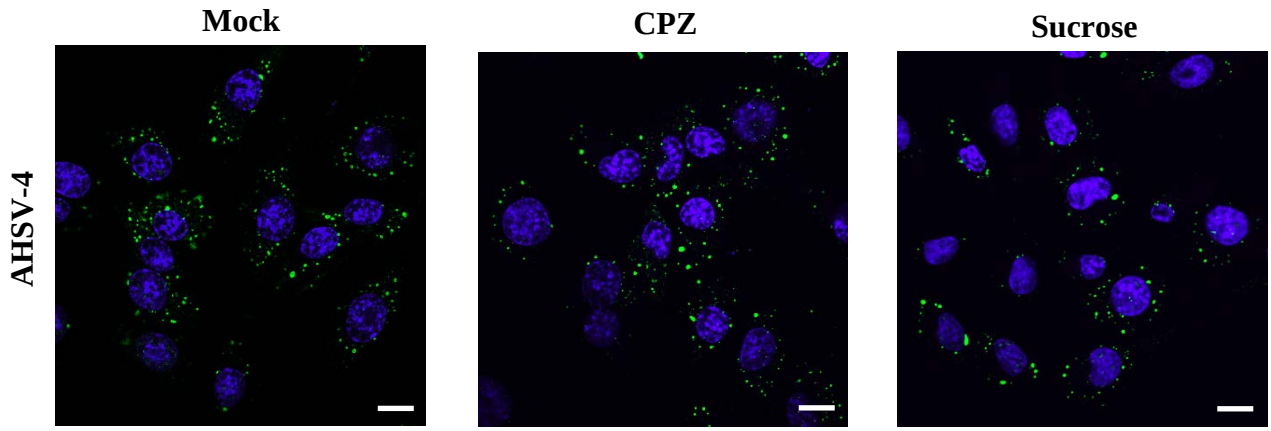
Mock
CPZ
Sucrose
AHSV-4

C

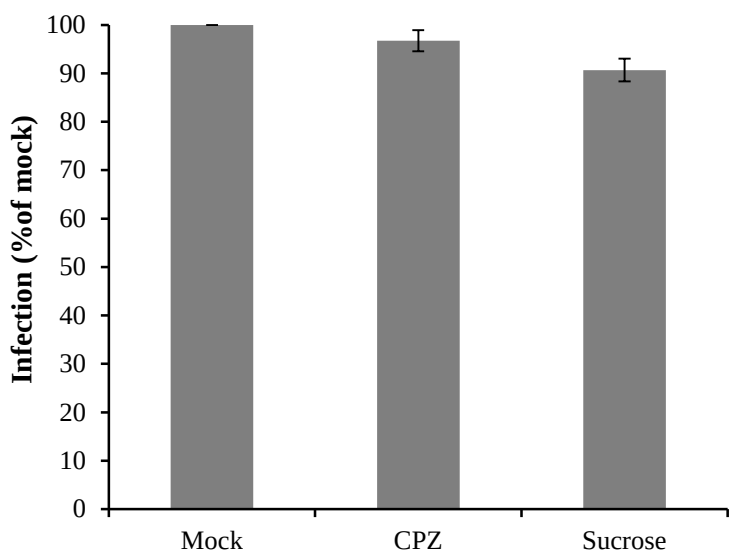
Infection (%of mock)
100
90
80
70
60
50
40
30
20
10
0
Mock
CPZ
Sucrose

D

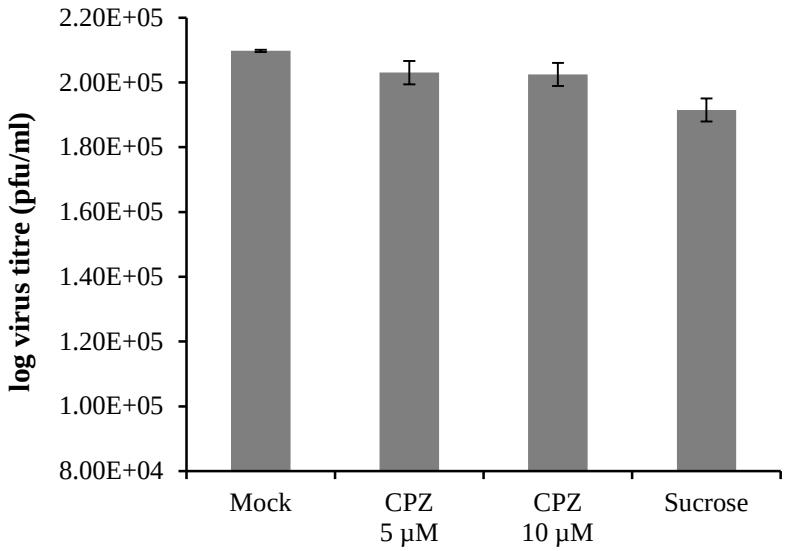
2.20E+05
2.00E+05
1.80E+05
1.60E+05
1.40E+05
1.20E+05
1.00E+05
8.00E+04
log virus titre (pfu/ml)
Mock
CPZ 5 µM
CPZ 10 µM
Sucrose

E

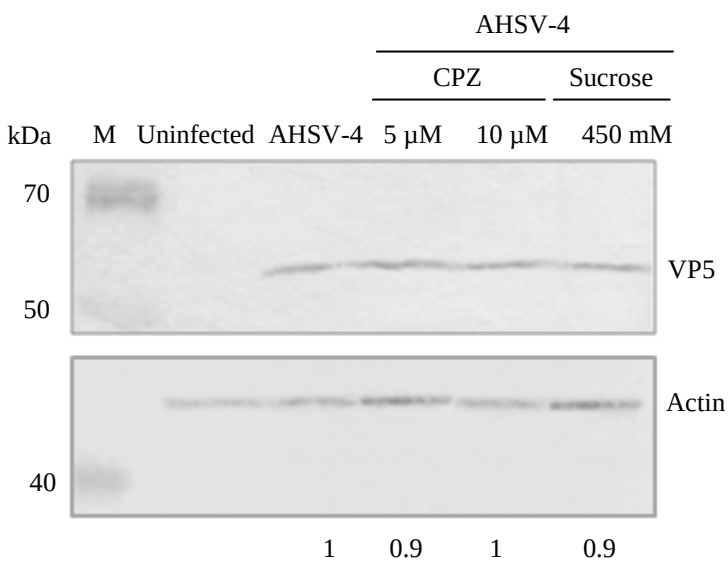
AHSV-4
CPZ
Sucrose
kDa
M
Uninfected
AHSV-4
5 µM
10 µM
450 mM
70
50
40
VP5
Actin
1
0.9
1
0.9

Figure 2

A

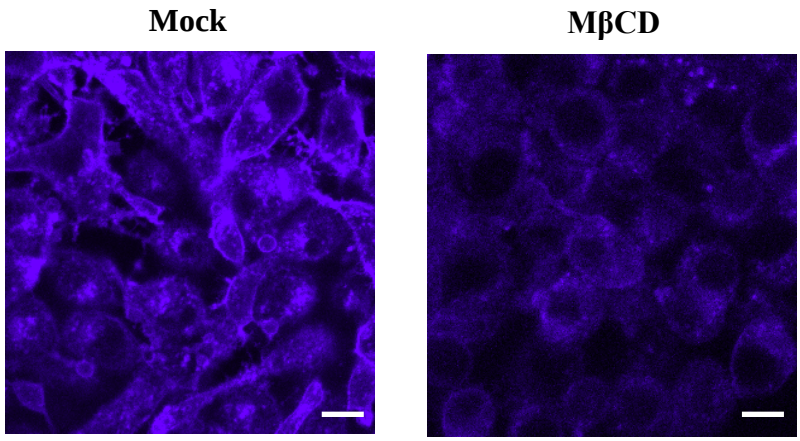
Mock
MβCD

B

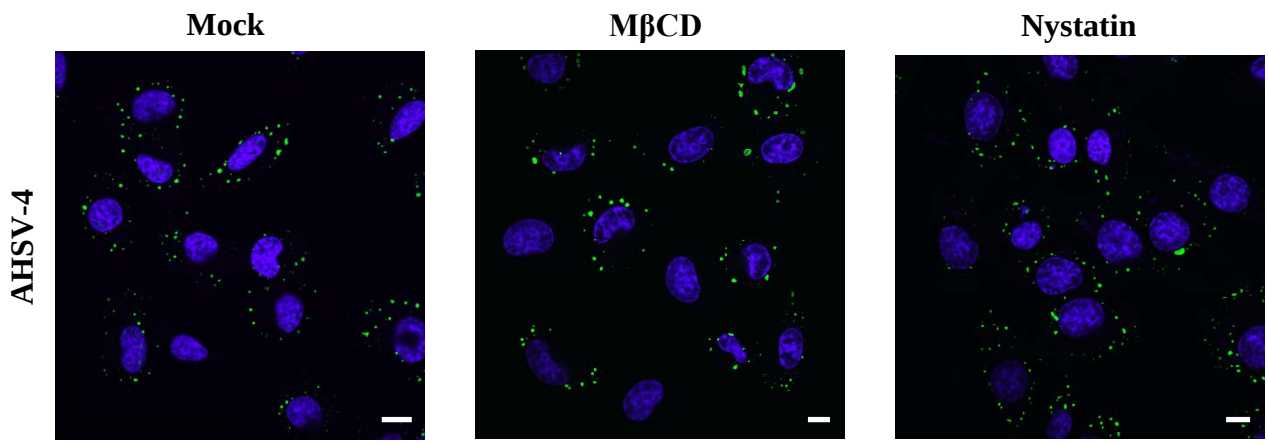
Mock
MβCD
Nystatin
AHSV-4

C

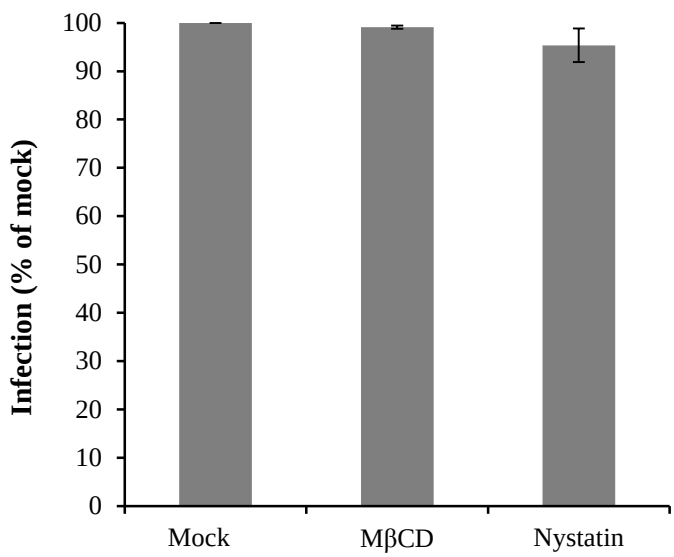
Infection (% of mock)
100
90
80
70
60
50
40
30
20
10
0
Mock
MβCD
Nystatin

D

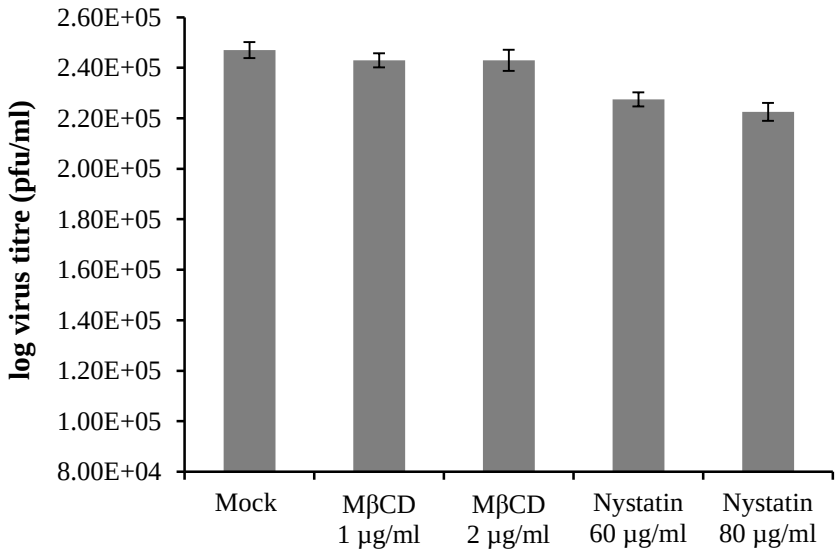
log virus titre (pfu/ml)
2.60E+05
2.40E+05
2.20E+05
2.00E+05
1.80E+05
1.60E+05
1.40E+05
1.20E+05
1.00E+05
8.00E+04
Mock
MβCD 1 µg/ml
MβCD 2 µg/ml
Nystatin 60 µg/ml
Nystatin 80 µg/ml

E

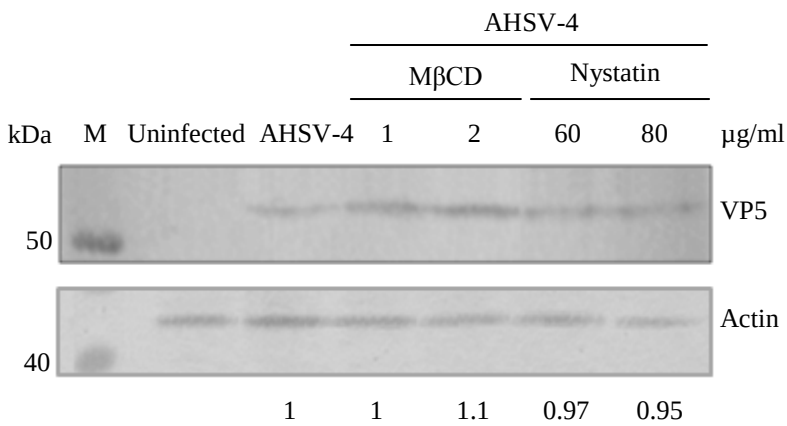
AHSV-4
MβCD
Nystatin
kDa
M
Uninfected
AHSV-4
1
2
60
80
µg/ml
50
VP5
40
Actin
1
1
1.1
0.97
0.95

Figure 3

A

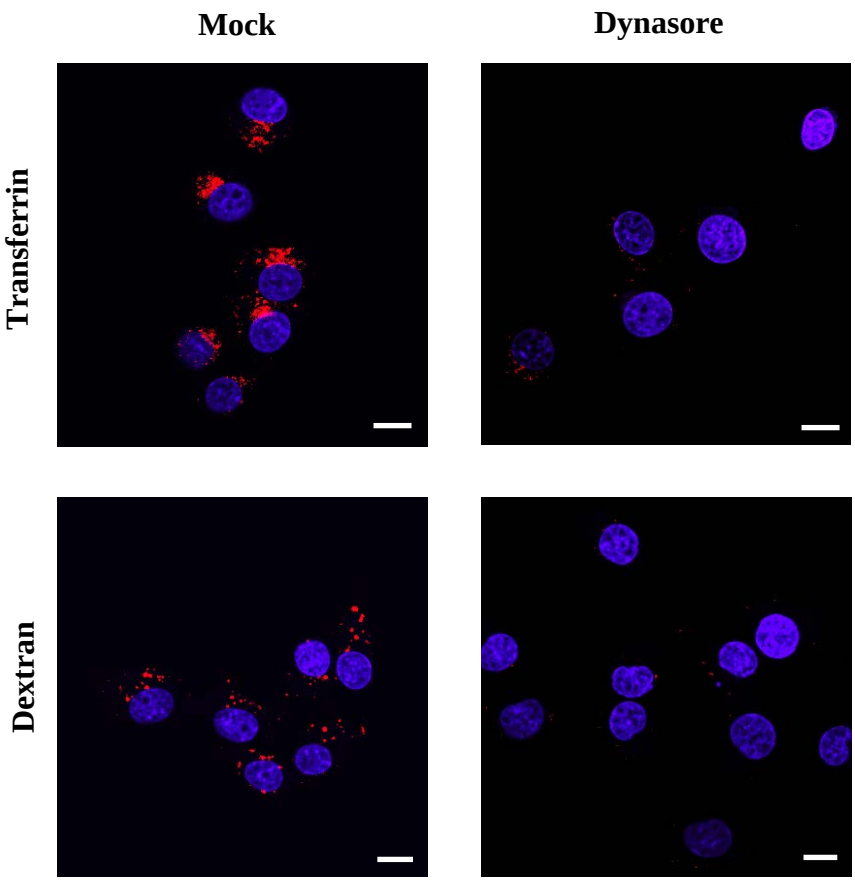

B

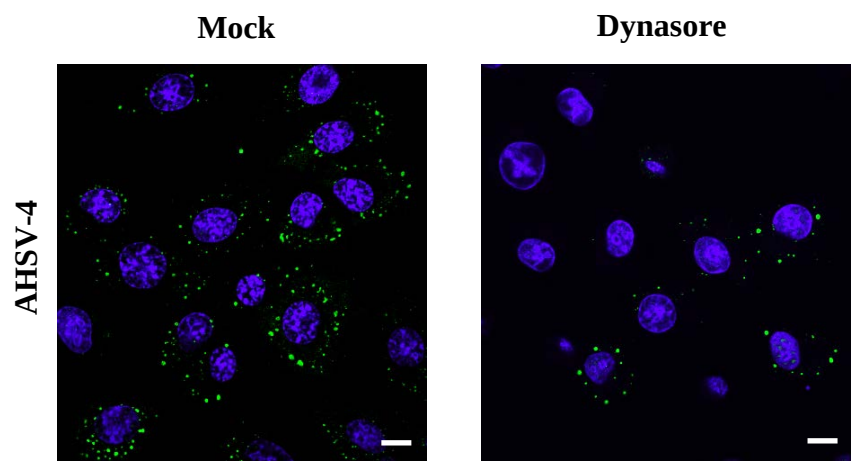

C

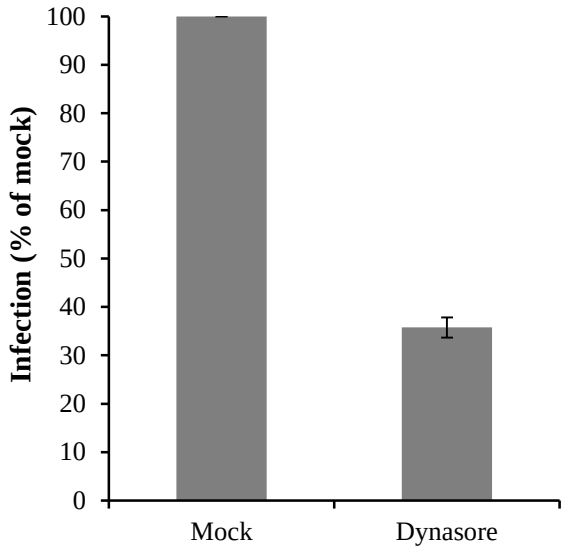
Infection (% of mock)
100
90
80
70
60
50
40
30
20
10
0
Mock
Dynasore

D

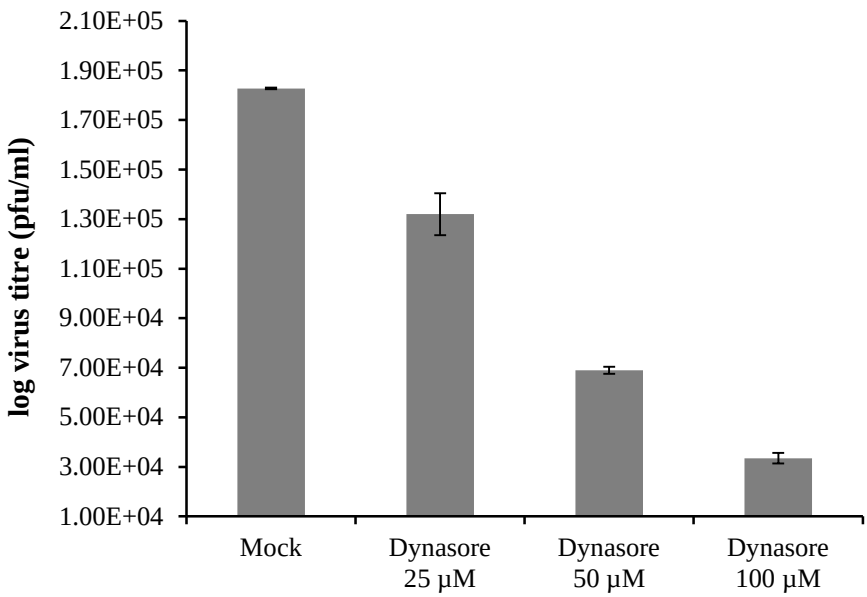
log virus titre (pfu/ml)
2.10E+05
1.90E+05
1.70E+05
1.50E+05
1.30E+05
1.10E+05
9.00E+04
7.00E+04
5.00E+04
3.00E+04
1.00E+04
Mock
Dynasore 25 µM
Dynasore 50 µM
Dynasore 100 µM

E

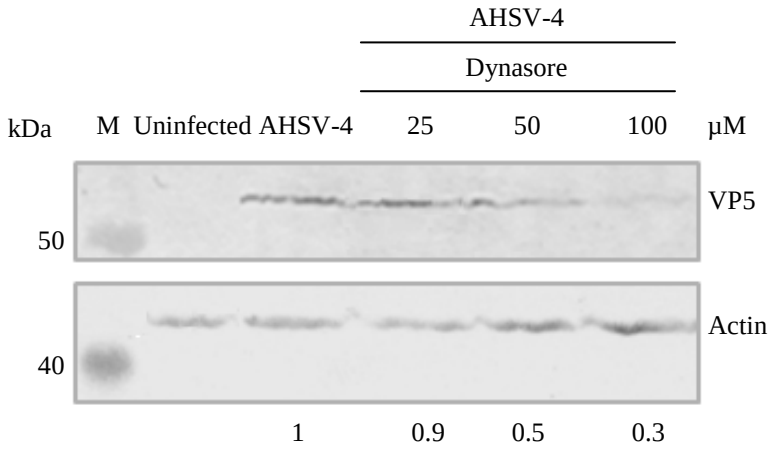
AHSV-4
Dynasore
kDa
M
Uninfected
AHSV-4
25
50
100
μM
50
VP5
40
Actin
1
0.9
0.5
0.3

Figure 4

A

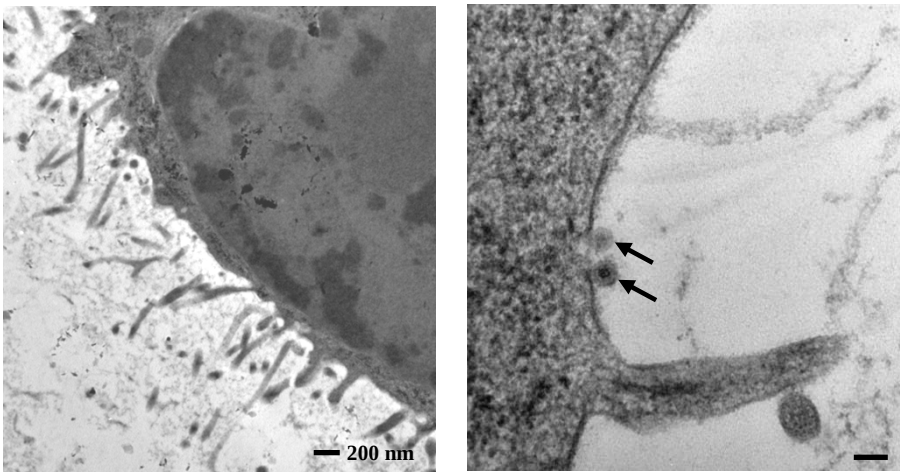

B

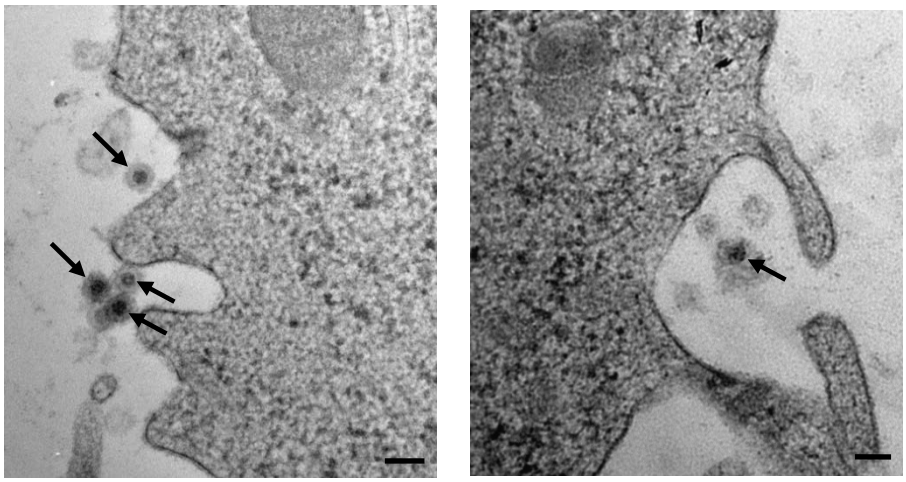

C

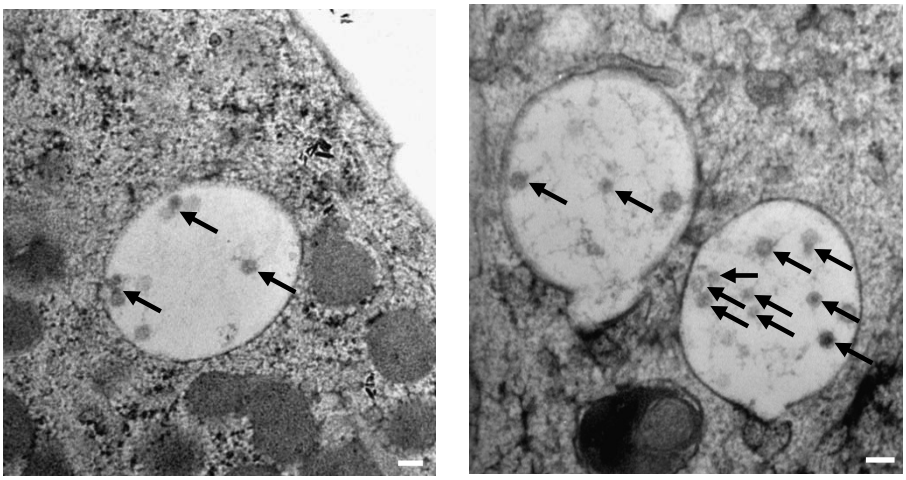

D

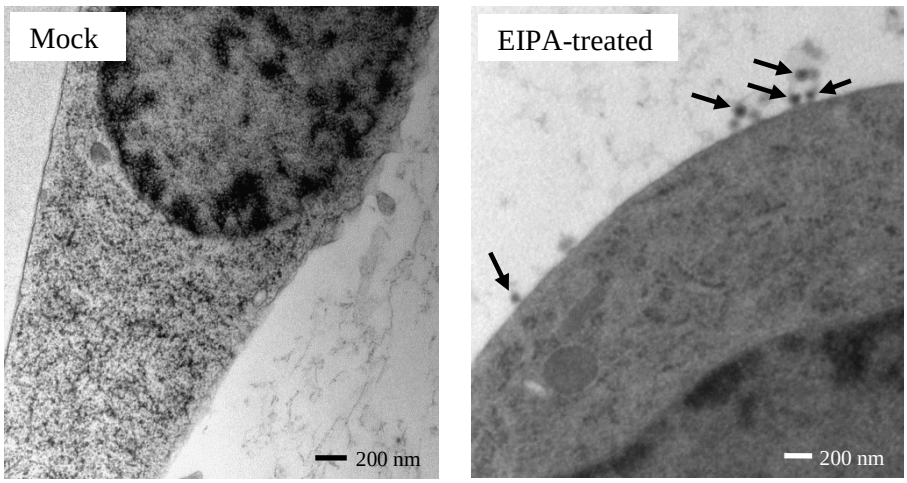

E

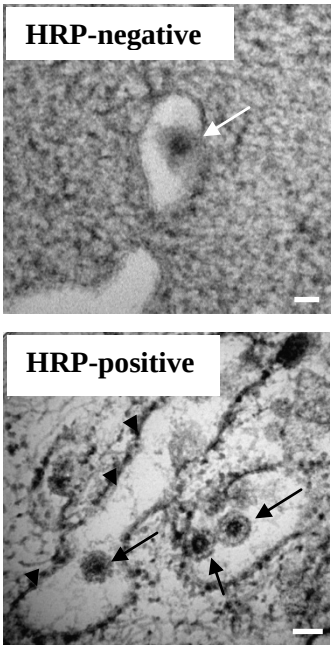
HRP-negative
HRP-positive

F

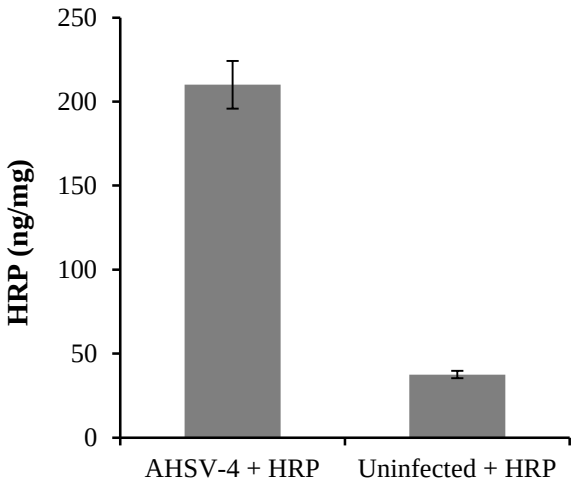
HRP (ng/mg)
250
200
150
100
50
0
AHSV-4 + HRP
Uninfected + HRP

Figure 5

A

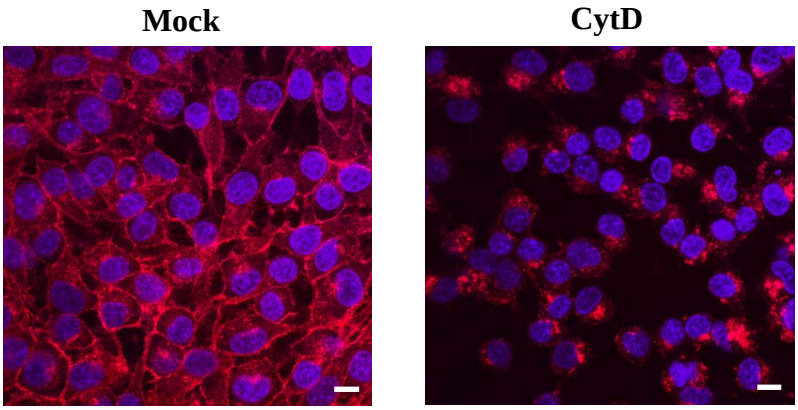
Mock
CytD

B

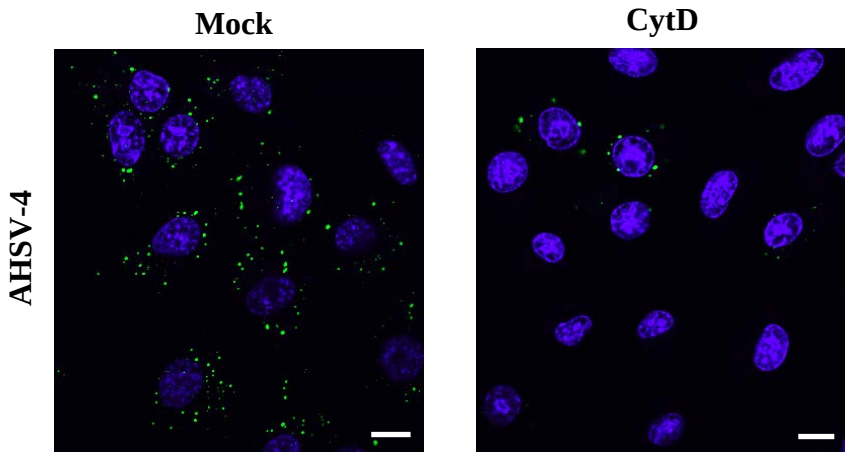
Mock
CytD
AHSV-4

C

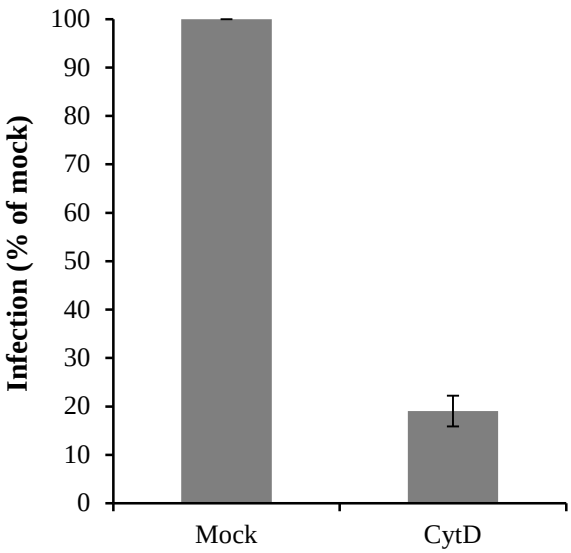
Infection (% of mock)
100
90
80
70
60
50
40
30
20
10
0
Mock
CytD

D

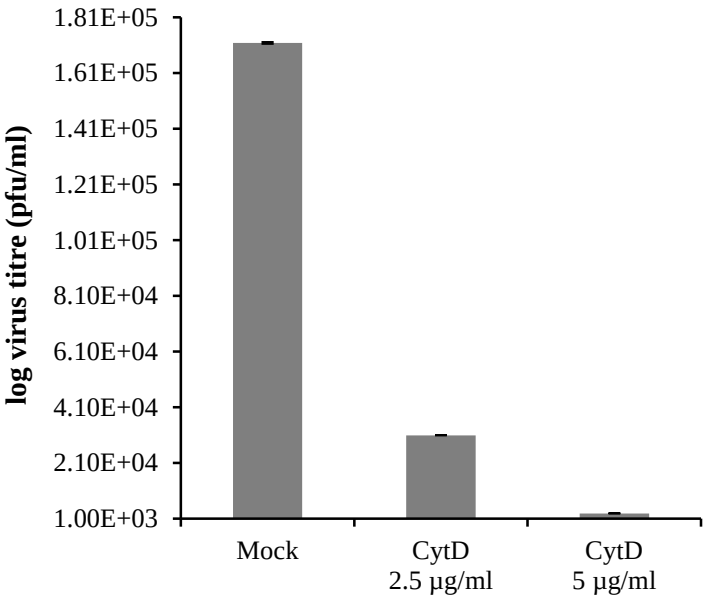
log virus titre (pfu/ml)
1.81E+05
1.61E+05
1.41E+05
1.21E+05
1.01E+05
8.10E+04
6.10E+04
4.10E+04
2.10E+04
1.00E+03
Mock
CytD 2.5 µg/ml
CytD 5 µg/ml

E

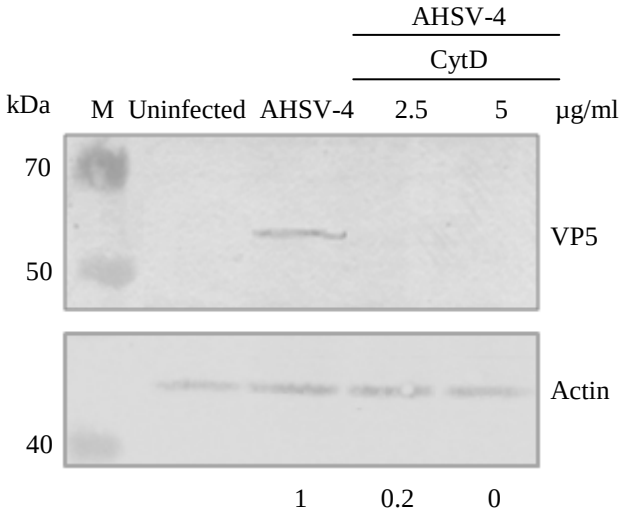
AHSV-4
CytD
kDa
M
Uninfected
AHSV-4
2.5
5
µg/ml
70
50
40
VP5
Actin
1
0.2
0

Figure 6

A

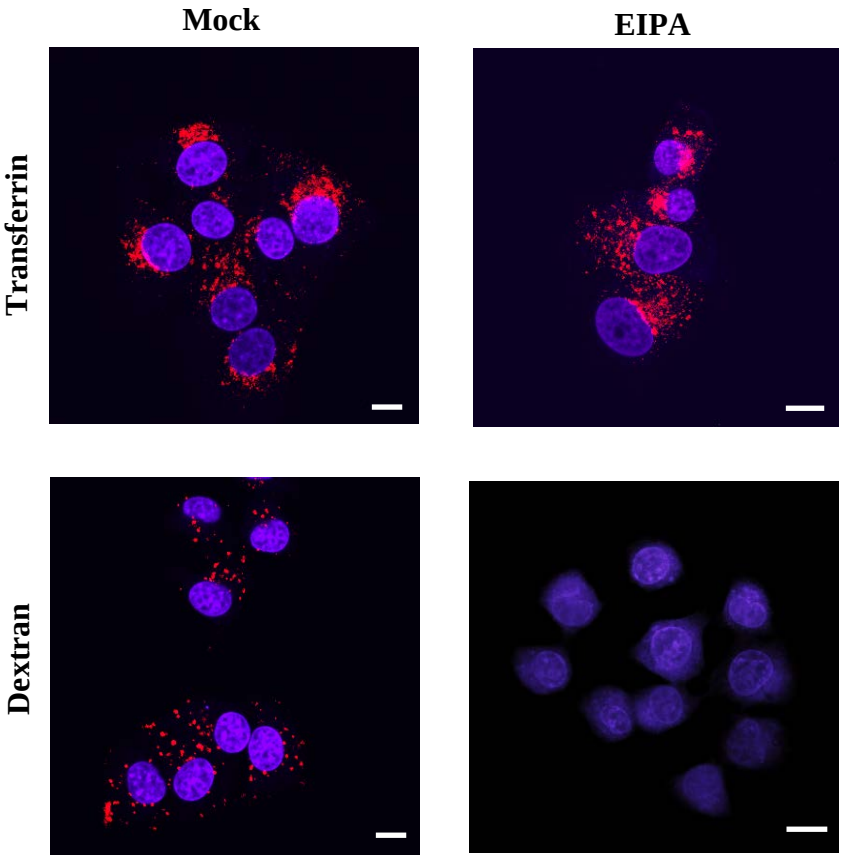

B

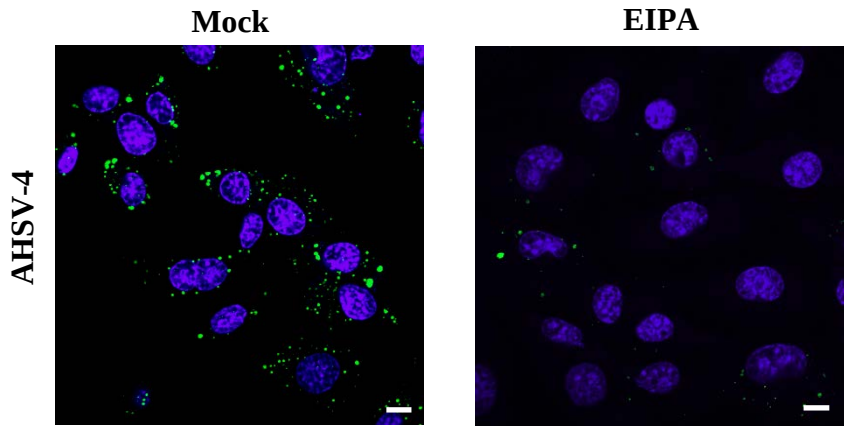

C

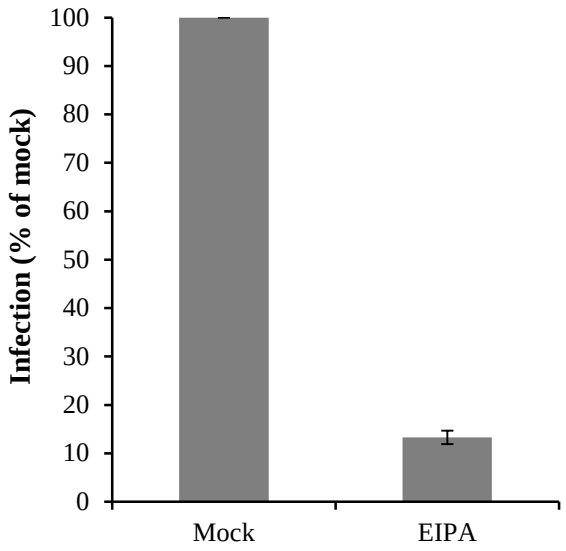
Infection (% of mock)
100
90
80
70
60
50
40
30
20
10
0
Mock
EIPA

D

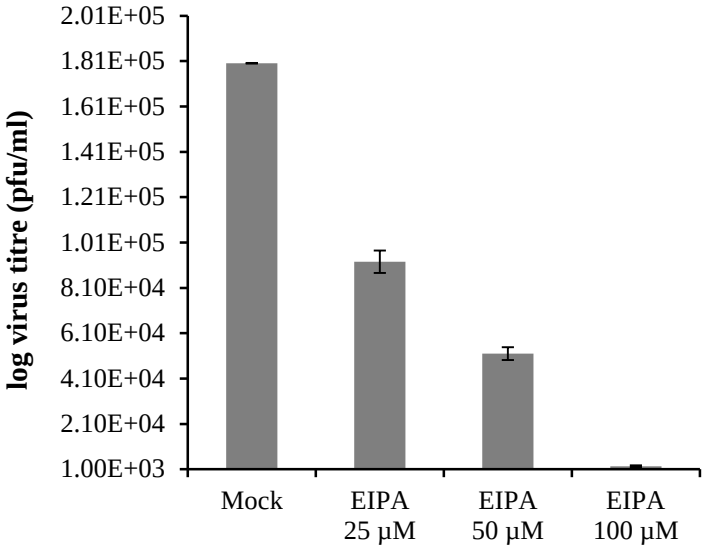
log virus titre (pfu/ml)
2.01E+05
1.81E+05
1.61E+05
1.41E+05
1.21E+05
1.01E+05
8.10E+04
6.10E+04
4.10E+04
2.10E+04
1.00E+03
Mock
EIPA 25 µM
EIPA 50 µM
EIPA 100 µM

E

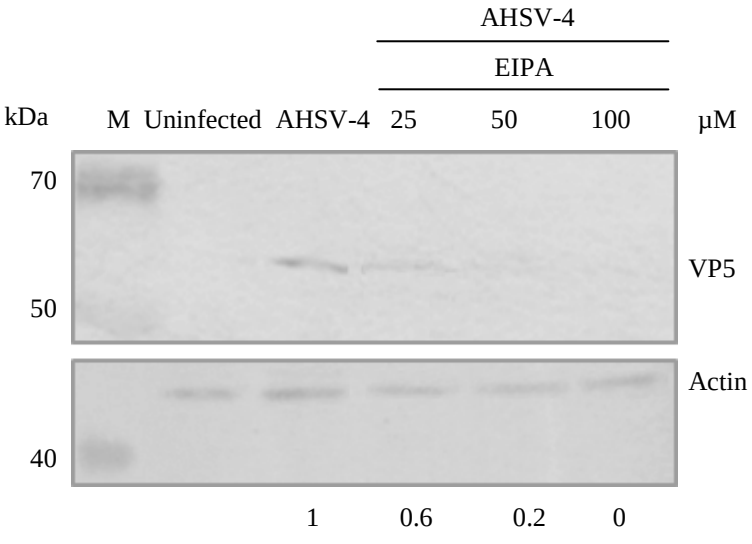
AHSV-4
EIPA
kDa
M
Uninfected
AHSV-4
25
50
100
µM
70
50
40
VP5
Actin
1
0.6
0.2
0

Figure 7

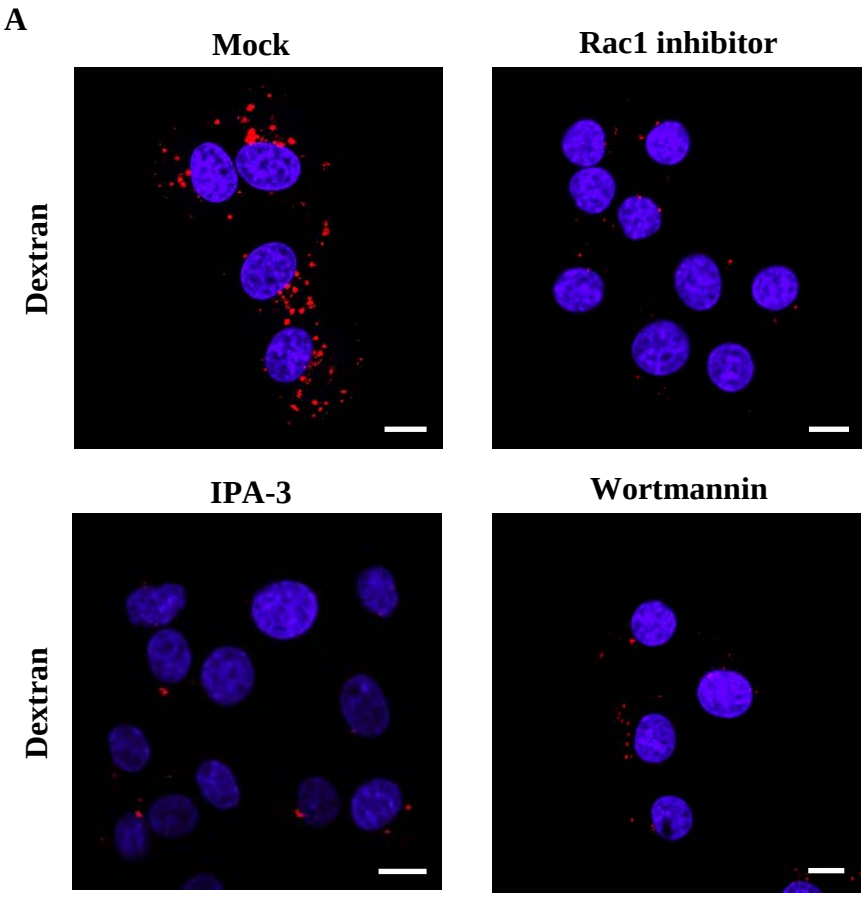
A
Mock
Rac1 inhibitor
Dextran
IPA-3
Wortmannin
Dextran

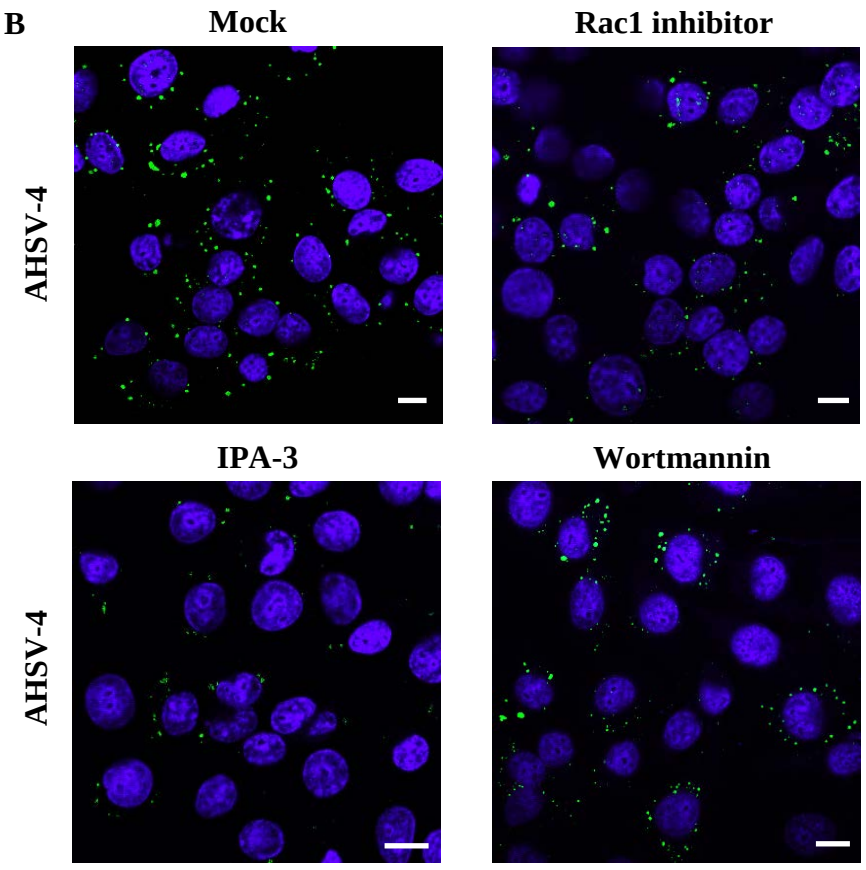
B
Mock
Rac1 inhibitor
AHSV-4
IPA-3
Wortmannin
AHSV-4

C

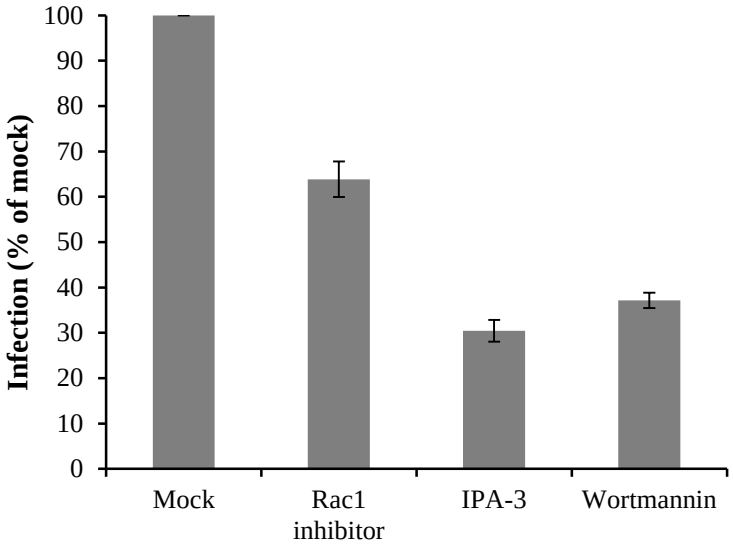
Infection (% of mock)
100
90
80
70
60
50
40
30
20
10
0
Mock
Rac1 inhibitor
IPA-3
Wortmannin

D

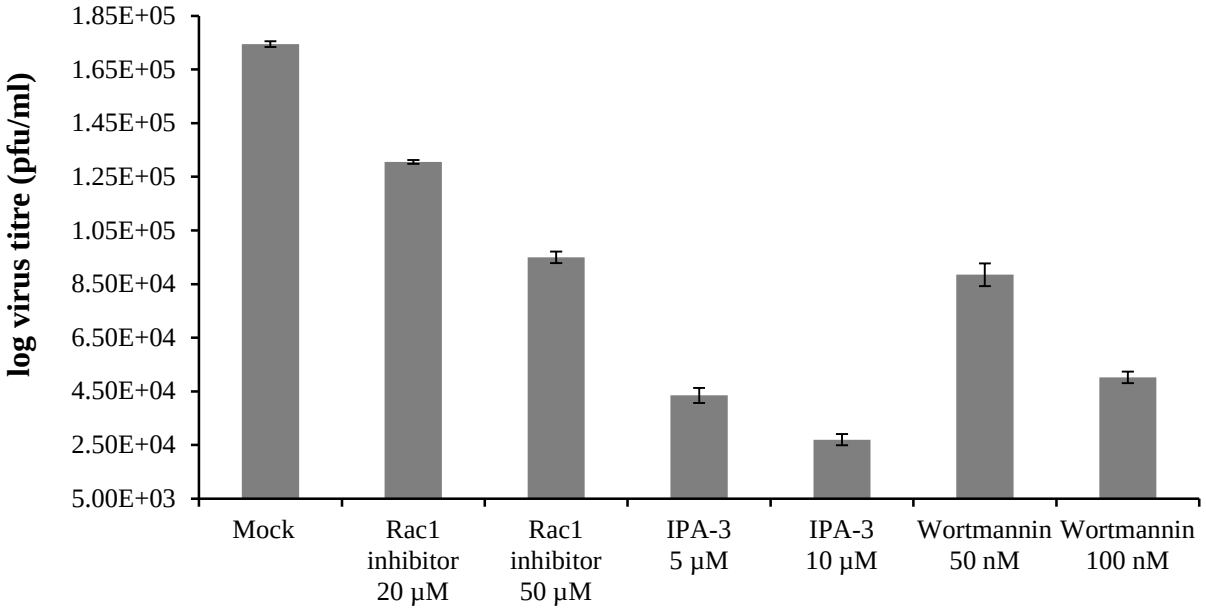
log virus titre (pfu/ml)
1.85E+05
1.65E+05
1.45E+05
1.25E+05
1.05E+05
8.50E+04
6.50E+04
4.50E+04
2.50E+04
5.00E+03
Mock
Rac1 inhibitor 20 µM
Rac1 inhibitor 50 µM
IPA-3 5 µM
IPA-3 10 µM
Wortmannin 50 nM
Wortmannin 100 nM

E

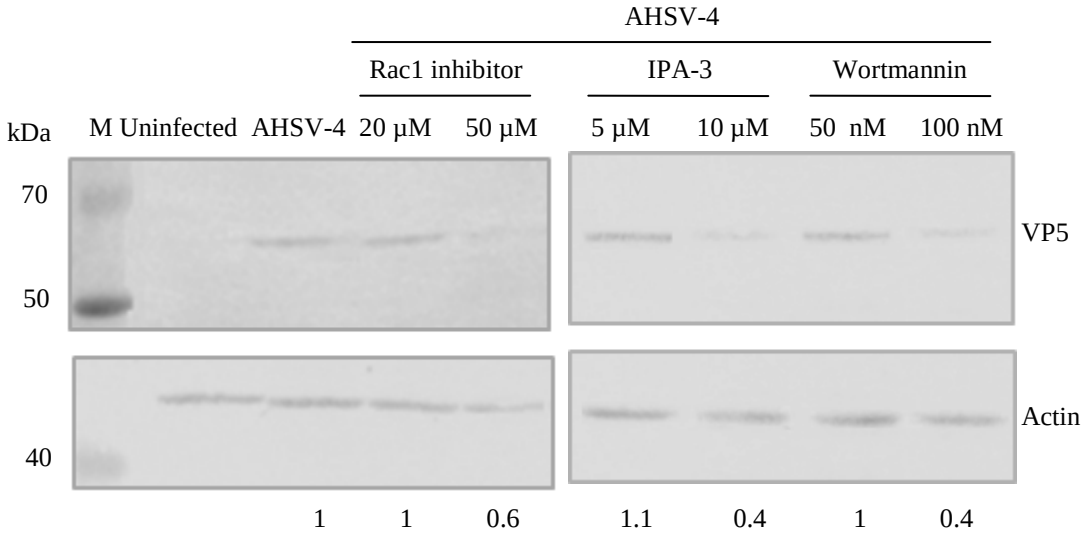
AHSV-4
Rac1 inhibitor
IPA-3
Wortmannin
kDa
M
Uninfected
AHSV-4
20 μM
50 μM
5 μM
10 μM
50 nM
100 nM
70
50
40
VP5
Actin
1
1
0.6
1.1
0.4
1
0.4

Figure 8

Supplementary material

A

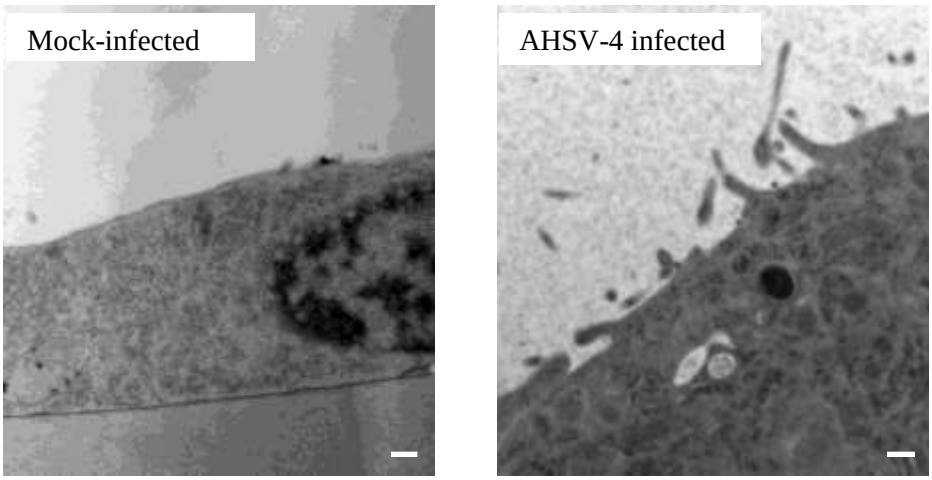

B

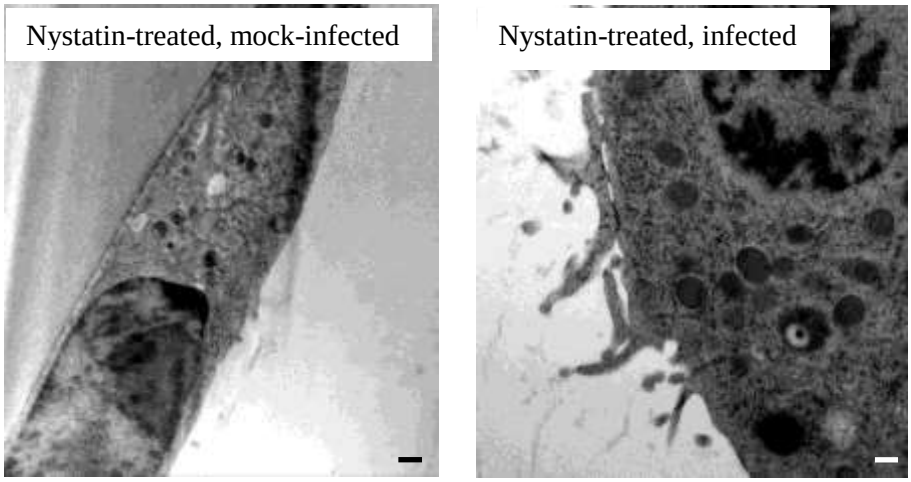

C

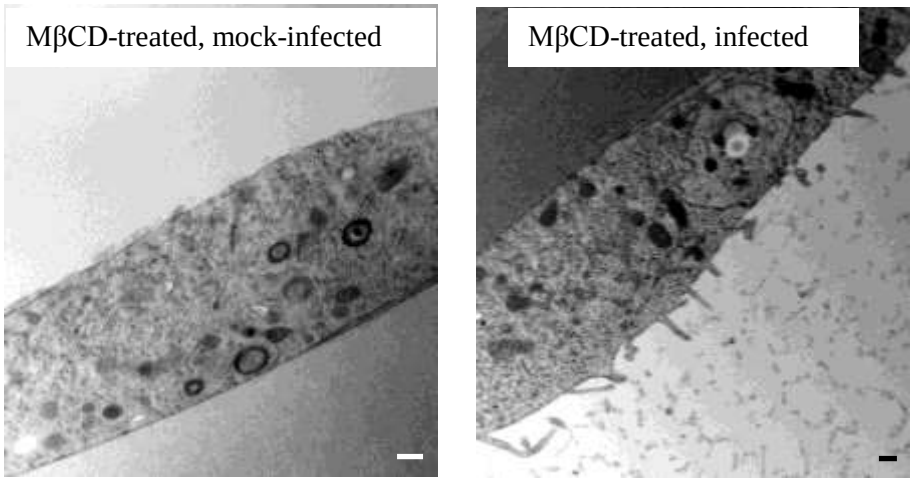

Supplementary Fig. S1. Membrane ruffling occurs in BSR cells infected with AHSV-4 in the presence of nystatin or MβCD, but does not occur in mock-infected treated control cells. (A) AHSV-4 infection induced plasma membrane ruffling, whereas no membrane ruffling was observed in mock-infected BSR cells. (B-C) No membrane ruffling was observed in mock-infected BSR cells treated with either nystatin (80 µg/ml) or MβCD (2 µg/ml), whereas membrane ruffling was induced upon infection with AHSV-4 in the presence of nystatin or MβCD. Scale bars = 200 nm.

Supplementary Table S1: Viability of drug-treated BSR cells

Drug	Concentration tested	Cell viability (%)
Ammonium chloride	0	100
	10 mM	99
	25 mM	98
	50 mM	84
	100 mM	74
Chloroquine	0	100
	100 µM	100
	200 µM	99
	300 µM	91
	500 µM	85
Chlorpromazine	0	100
	5 µM	100
	10 µM	99
	25 µM	75
	50 µM	45
Methyl-β-cyclodextrin	0	100
	1 µg/ml	100
	2 µg/ml	100
	5 µg/ml	85
	10 µg/ml	77
Nystatin	0	100
	40 µg/ml	100
	60 µg/ml	100
	80 µg/ml	100
	100 µg/ml	80
Dynasore	0	100
	25 µM	100
	50 µM	99
	100 µM	98
	150 µM	52
Cytochalasin-D	0	100
	1 µg/ml	100
	2.5 µg/ml	100
	5 µg/ml	97
	10 µg/ml	58
EIPA	0	100
	25 µM	100
	50 µM	99
	100 µM	98
	150 µM	71
Rac1 inhibitor	0	100
	10 µM	98
	20 µM	97
	50 µM	97
	80 µM	81
IPA-3	0	100
	2 µM	100
	5 µM	99
	10 µM	97
	15 µM	84

Wortmannin	0	100
	25 nM	100
	50 nM	98
	100 nM	97
	125 nM	89